Migration and Abundance of Bigeye Tuna (*Thunnus obesus*), and Other Pelagic Species, Inferred from Catch Rates and Their Relation to Variations in the Ocean Environment

Patrick Hyder
1 Met Office, Fitzroy Road
Exeter EX1 3PB
United Kingdom

Keith Bigelow, Russell Brainard,
Michael Seki, and June Firing
NOAA National Marine Fisheries Service
2570 Dole Street, Honolulu HI 96822

Pierre Flament
School of Ocean and Earth Science and Technology
University of Hawaii, Honolulu HI 96822

SOEST 09-02
JIMAR Contribution 09-371

Acknowledgements

The Pelagic Fisheries Research Program funded this research through the project "The Role of Oceanography on Bigeye Tuna Aggregation and Vulnerability in the Hawaii Longline Fishery from Satellite, Moored, and Shipboard Time Series". Dave Itano and John Gunn kindly provided tag data. The NOAA Ship *Ka'imimoana* and her crew undertook all the mooring operations at no cost to the project, courtesy of Dr. Michael McPhaden (NOAA/PMEL) and the TAO project. Eric Firing provided valuable technical input for the analysis of ADCP observations and provided access to archived ship-mounted ADCP data. Ole Smedstad at the Naval Research Laboratory provided simulations from the NLOM model for comparison with the mooring observations. John Sibert provided valuable discussion. Gary Mitchum provided processed along-track altimeter sea surface height anomaly data. Peter Hacker provided technical information on ocean models, which were obtained from the Asia Pacific Data Research Centre data server. Dave Foley and Lucas Moxey provided NOAA satellite observations. Donald Kobayashi compiled catch rate data for the Hawaii-based longline fishery.

Abstract

Bigeye tuna catch rates vary on a variety of temporal and spatial scales, including inter-annual, associated with the El Niño–Southern Oscillation (ENSO); seasonal, associated with the annual temperature cycle; and mesoscale, associated with ocean mesoscale variability including eddies. Bimonthly averages of latitudinal variation in effort, catch, and catch rate (CPUE) are compared with environmental parameters. The results suggest a broad annual migration strongly influenced by the preferred near surface temperature range. The region of maximum relative abundance in the northern hemisphere migrates from subtropical waters in September when these waters are warmest to tropical waters in March when subtropical waters are coldest. The inferred migration is supported by north-south annual migration of the catch rate center of mass (COM). However, the latitudinal CPUE variations also indicate that the fish venture to regions outside their preferred thermal ranges for short times. The Secretariat of the Pacific Community (SPC) and Japanese Pacific data sets indicate similar Pacific-wide variations for bigeye. Latitudinal catch rate analyses and CPUE COM seasonal latitudinal variations suggest significant seasonal north-south catch rate migrations may also occur for other pelagic species.

Table of Contents

List of Figures

1. INTRODUCTION

Fishermen have been aware of the migratory nature of the worldwide tuna fishery for many years and adjusted their fishing effort accordingly. The management and assessment of stocks of highly migratory species pose problems for both scientists and managers alike because of migration of the fish into and out of different regions. It is essential to maximize our comprehension of how changes in the environment affect the horizontal and vertical distribution of fish and their catchability through gear performance; combined, they result in the catch rates that are used in stock assessment.

Bigeye tuna (*Thunnus obesus*) has been the main target species of the longline fishery in the tropical and subtropical Pacific since the introduction of the "deep" longline technique in the Japanese longline fishery during the mid-1970s. The importance of the bigeye longline fishery grew during the 1990s as the number of longline vessels increased in Hawaii, French Polynesia, Australia, and other Pacific Island states. Pacific-wide catches over the last decade have varied between approximately 150,000 and 180,000 tons (Hampton et al., 1999). Stock assessments have been conducted using indices of abundance, non-equilibrium production models, cohort analysis, and yield-per-recruit analysis (Miyabe, 1995; Hampton et al., 1998; and IATTC, 1999). Central to each method is the use of longline fishery catch and effort statistics to construct indices of abundance based on catch rate. Recent stock assessments of bigeye tuna have indicated a decline since the year 2000 to current low levels of ~600,000 tons (Maunder and Hoyle, 2006; Hampton et al., 2005; Sibert et al., 2006). With fishing at a high level compared to the total stock biomass, it is essential to obtain accurate estimates of stock. This requires an accurate understanding of the relation between catch rate and abundance.

The catch of bigeye tuna is strongly influenced by the depth of the gear, with gear used at greater depths being generally more effective in catching bigeye (Hanamoto, 1987; Boggs, 1992; and Brill and Lutcavage, 2001). Prior to 1970, effort was largely conventional sets (5–6 hooks between floats, HBF) fishing to a depth range of approximately 90–150 m (Suzuki, *et al*., 1977; Bigelow et al., 2002). However, since that time there has been a shift to deep sets (> 10 HBF), in which the majority of hooks are in the depth range 100–250 m. This switch has increased the effectiveness of longline gear, with greater gains in the western and central Pacific where the pycnocline is generally deeper. The bigeye preference for certain thermal conditions, in combination with their physiological minimum oxygen concentration limitations, and their tendency to feed in the scattering layer concentrates the fish vertically, particularly in equatorial waters in the western Pacific where the oxycline is shallow (Bigelow et al., 2002).

In this report, we focus on horizontal changes in catch rates. We attempt to use seasonal migrations of catch rate to infer migrations of fish. Details of the methods and data employed in the analyses are presented in Section 2. We make the basic assumption that over the time and length scales considered, the systematic changes in abundance per unit area are larger than the changes in catchability and, hence, catch rates depend principally on abundance. We discuss the validity of this assumption for seasonal variations in Section 3. Section 3 also includes background analyses and review, including a review of bigeye tuna, a first-order assessment of the expected relative magnitudes of expected seasonal vertical and spatial catch rate variations, and a review of

the oceanography of Hawaiian Islands region. Section 4 presents the results of the catch rate analyses. Finally, in Section 5, we discuss our results.

2. METHODS

2.1 Catch Rate Data

The Hawaii-based longline fishery targeting bigeye tuna extends from equatorial waters close to Palmyra to the waters to the north of the main Hawaiian Islands around 35°N. Data presented in this paper cover the 12-yr period from November 1990 to September 2002. Data are collected by captains of the longline vessels that make up the Hawaii-based longline fleet and are compiled at the National Oceanic and Atmospheric Administration (NOAA) National Marine Fisheries Service (NMFS). Locations given are mean locations from start of haul, end of haul, start of set, and end of set. For this analysis, the data were filtered to include only deep longline sets consisting of more than 10 HBF, which means that generally 90% of the hooks are at depths > 100 m. No data were collected either on fish size (which is recorded separately by the auction house) or the hook number relative to the float at which the catch occurred. The region was gridded by 1° latitude and longitude squares for analyses of spatial variations and in 2° squares for the latitudinal (North/South) sections. Time is in days beginning on 1 January 1990. For seasonal and interannual plots, times are presented in number and fractions of the year (years are approximated in blocks of 365 days beginning on 1 January 1990).

For the Pacific-wide analysis, we analyzed CPUE or catch rate (defined as fish per thousand hooks) data for several pelagic species, including bigeye tuna in 5° latitude and longitude squares for the Japanese longline fleet (1975−2001) and SPC all-fleet Pacific longline data (1970–2000). For the Japanese longline data, all effort categories were included in the analyses because differences between the effort categories were not found to be significant for bigeye. Pacific-wide CPUE or catch rate data were not compared individually with environmental parameters because the exact locations of individual catches were not available.

To estimate the mean position of the CPUE, we used a COM parameter. This simply represents the mean position weighted according to the parameter chosen. For a parameter, n, for latitude and longitude these are simply given by:

$$\mathrm{COM}_{\mathrm{lat}} = \Sigma\,(n^{*}\mathrm{lat}_n) \,/\, \Sigma\,(n) \qquad \mathrm{COM}_{\mathrm{lon}} = \Sigma\,(n^{*}\mathrm{lon}_n) \,/\, \Sigma\,(n). \qquad (1)$$

2.2 Environmental Data

Comparisons between catch rate and oceanographic parameters were conducted for the Hawaii-based longline fishery using satellite-derived surface parameter data and simulated temperature data from the JPL ECCO assimilative model. For comparison with Pacific equatorial catch rate data we used the Simple Ocean Data Assimilation (SODA) data because it covered the full period from 1950 to 1999. The data sets used for each analysis are stated when the results are discussed (or included in figure captions).

The JPL ECCO-2 employs the Massachusetts Institute of Technology Global Circulation Model for a near-global domain (78°S~78°N). Model resolution is 1° horizontally except within the tropics where meridional resolution gradually decreases to

~0.3° within 10° of the Equator. The model is forced by National Centre for Environmental Prediction (NCEP) reanalysis products (12-hourly wind stress, daily adiabatic air-sea fluxes) with time-means replaced by those of the Comprehensive Ocean-Atmosphere Data Set (COADS). Temperature and salinity at the model sea surface are relaxed towards observed values. Averaged model fields are available at 10-day intervals. Sea level anomalies (TOPEX/Poseidon) are assimilated into the model using a Kalman filter (Fukumori, 2002). Thermal data to 700 m along a section at 161.5°W from the JPL ECCO model were extracted from the IPRC data server at 2.5° intervals between 0.0°N and 37.5°N. Although there are several versions of SODA (Carton et al., 2005), the version we use (1.4.2) is forced by European Centre for Medium-range Forecasts (ECMWF) winds from 1958 to 2001. The ocean model is based on Parallel Ocean Program physics with an average 0.25° × 0.4° with a 40-level resolution (Carton et al., 2005). Observations used for the analysis include virtually all available hydrographic profile data as well as ocean station data, moored temperature and salinity time series, surface temperature and salinity observations of various types, and nighttime infrared satellite SST data. The output is in monthly-averaged form, mapped on a uniform 0.5° × 0.5° × 40-level grid. The Naval Research Laboratory (NRL) Layered Ocean Model (NLOM) with 1/16° horizontal resolution was used for comparison of simulated oceanographic parameters both with mooring observations and with spatial variations in catch rate in the Hawaiian Islands region, which are included in Appendix 1. This model with seven layers of varying thickness assimilates satellite-derived sea surface temperature (SST) and height observations using an optimal interpolation technique (Smedstad et al., 2002).

2.2.1 Satellite-Derived SST from the NOAA Advanced Very High Resolution Radiometer (AVHRR) and Ocean Color from NASA SEAWIFS Projects

Satellite-derived SST from the NOAA Advanced Very High Resolution Radiometer (AVHRR) and ocean color from NASA SEAWIFS Projects are interpolated into weekly composites at NOAA NMFS. The sea level anomaly along track was observed by the altimeter aboard TOPEX/POSEIDON (T/P). We use the interpolated product from the AVISO laboratory, France (http://www.aviso.oceanobs.com). The along-track data and AVISO products are referenced to mean sea level and have tides and inverse barometer variations removed. The AVISO sea level anomaly was added to local mean sea level derived from NODC profile Levitus data to obtain an estimate for absolute sea level. In satellite-derived, gridded sea surface elevation data there will be interpolation errors associated both with the spatial averaging of the along track data onto the 0.25° grid and the temporal averaging of the 10-daily TOPEX cycle into the weekly composites. In particular, these interpolation errors may result in variations in the form of mesoscale features as they propagate across the satellite track lines, which are not real. Thus, for mesoscale analysis these data should be treated with caution. Second derivatives of interpolated products are subject to particularly large errors. Along track satellite-derived observations of mean sea level used in Appendix 1 were kindly provided by Gary Mitchum. Observations of subsurface temperature and salinity were derived from the National Ocean Data Centre (NODC) 2001 World Ocean Atlas climatology. Subsurface chlorophyll observations are from those available in 2003 from the NODC database.

Surface currents were estimated from observed surface height anomalies or from horizontal internal pressure gradients calculated from subsurface density variations in the upper water column (i.e., dynamic height) by assuming geostrophic balance (Fu and Cazenave, 2001). For the dynamical height analysis we considered only the upper 1000 m and assumed horizontal pressure gradients at the base of this layer were zero (i.e., a level of no motion at 1000 m). Geostrophic currents do not include the wind forced Ekman transport component of the current, which is expected to be significant near the surface. Based on the complexity of estimating the vertical structure of Ekman transport (due to its dependence on the time-varying profile of eddy viscosity), we did not consider this contribution (although it is included in the NLOM model simulations).

Moored instrument observations between 700 m depth and the surface at a location in 4275 m water depth in the Hawaiian Lee (20.6°N 161.6°W) were conducted between December 1999 and December 2001. The in situ and satellite-derived observations warrant further consideration in a separate publication. However, preliminary results from the initial analyses are included in Appendix 1 to make them available to other researchers. These include: (i) variations in temperature and currents at the mooring location; (ii) the correlation between sea surface height, dynamic height, and isotherm depth at the mooring location; (iii) comparison between the observed sea level and dynamic height (and observed currents with geostrophic surface current estimates) at the mooring location; (iv) comparison between locations of high catch rates and a range of satellite and model derived oceanographic parameters; and (v) comparison between the observations and simulations from the NLOM model.

3. BACKGROUND ANALYSIS AND REVIEW

In this section, we present a review of bigeye tuna, an assessment of relative magnitudes of expected seasonal vertical and spatial variations in catch rates, and a review and brief analysis of the oceanography of the Hawaiian region.

3.1 Bigeye Tuna

Bigeye tuna are found between 40°N and 40°S with optimum foraging temperature between 10°C and 15°C and a minimum oxygen threshold of ~1–2 mg/l (Hanamoto, 1987). Their distribution and migration is discussed in Kume (1967), their age distribution and growth are considered by Sun et al. (2000), and an introduction to the effect of the oceanographic environment on tuna is presented by Sund et al. (1981). Studies show that bigeye tuna exhibit a distinctive diurnal dive cycle (Schaefer and Fuller, 2002; Musyl et al., 2003; Dagorn et al., 2000). Nighttime is spent in the warm upper layer of the water column, while daytime foraging dive behavior has been grouped into several classes. During Type 1, which is the predominant behavior, daytime is spent oscillating between foraging in the scattering layer that is usually close to the base of the pycnocline and returning to surface waters for short periods between dives. During Type 2 behavior the fish do not migrate diurnally but remain in the upper water column during the day. Additional behaviors include deep dives in excess of 1000 m that may be considered actions to escape predation, and surface association with FADS and floating objects (Itano and Holland, 2000).

During Type 1 behavior, both the dive depth and proportion of time spent at the surface appear to vary between locations, giving rise to considerable variations in the overall depth distribution (Gunn and Hampton, 2003; Musyl et al., 2002; Schaefer and Fuller, 2002). The depth of the dive is thought to normally coincide with the depth of the deep scattering layer (Betrand *et al*., 2002; Josse et al., 1998). This appears to be shallower in the morning and evening (Musyl et al., 2003) but also varies spatially, usually between around 250 and 500 m. At some locations, the dive duration of bigeye tuna appears to be shorter for deeper dives. For example, in Hawaiian waters (Musyl et al., 2003) dives in excess of 400 m are generally less than 1 hr in duration, while dives in equatorial waters (Schaefer and Fuller, 2002) are longer (3–4 hrs) and shallower (250–300 m). This variability in dive cycles results in considerable variations in the depth-time and temperature-time distributions for bigeye tuna between locations and seasons.

Bigeye tuna have a countercurrent vascular system that allows them to preserve inner body temperature during dives (Musyl et al., 2002; Brill et al., 2005). Archival tag data suggests that in the upper water column between dives (and at night) bigeye prefer a thermal range of 22–26°C (Bigelow et al., 2002). Evidence suggests the fish may return to this warmer water to warm blood and external tissue rapidly between dives. Brill et al. (2005) describe this characteristic as returning to warm surface waters for a "gulp of heat" (in an analogous manner to a marine mammal returning to the surface for a "gulp of air"). If this is the case, it is possible the dive cycle for bigeye tuna could become restricted for dives initiated outside their preferred upper water thermal range. The proportion of time spent in the warmer upper-water column during the day has been observed in the Coral Sea to be higher in the winter and spring months (Figure 1), when upper layer temperatures within this layer are coolest (and blood might be expected to take longer to warm between dives).

The principal physiological depth confinement for bigeye dives is thought to be oxygen at levels of around 2 mg/l, although during dives they can reach depths where ambient oxygen is less than 1.5 mg/l (Brill et al., 2005). In certain regions in the equatorial and western tropical Pacific, this may vertically confine bigeye to certain depths (Bigelow et al., 2002). Bigeye tuna appear also to have a preference for water temperatures greater than 8°C, although they are known to expose themselves to temperatures as low as 5°C for relatively short periods (Brill et al., 2005).

3.2 Assessing the Relative Magnitude of Spatial and Vertical Catch Rate Changes

To evaluate whether our earlier assumption that spatial changes in abundance are expected to generally be greater than spatial changes in catchability (arising mainly from vertical variations of fish in relation to hooks) is valid, it is necessary to briefly examine the potential effect of vertical confinement of fish on the relation between catch rate and abundance. For given fish densities per unit volume, $A_{vol}(z)$, (number of fish/m^3) at each depth, z (m), in a layer of thickness, dz (m), the spatial abundance, A_{sp}, (number of fish/m^2) is determined by the sum through depth of the fish density over the depth range in which the fish are confined physiologically, D_c:

$$A_{sp} = \Sigma\, A_{vol}(z)\, dz \qquad (2)$$

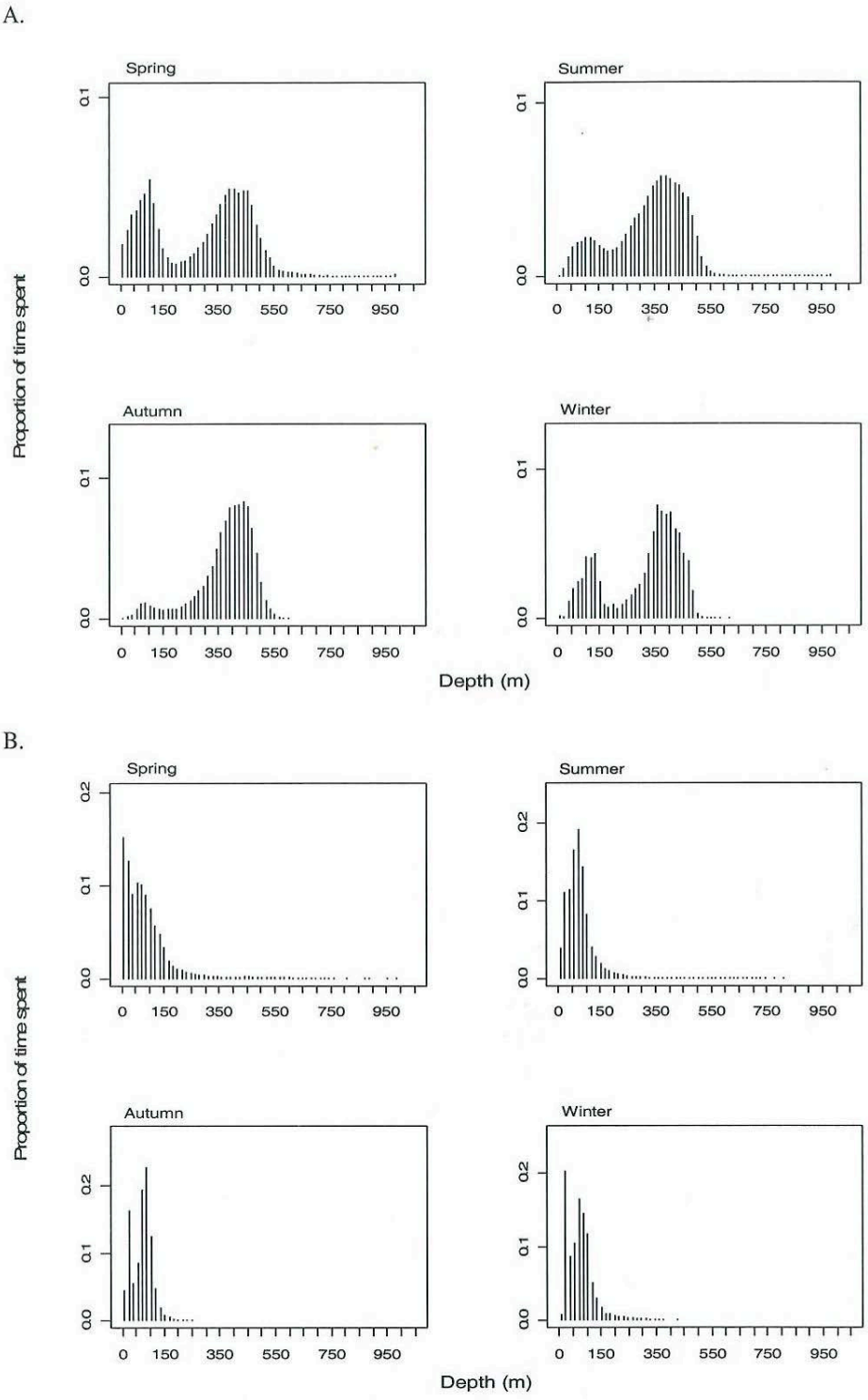

Figure 1. The vertical distribution of the fish as a proportion of time spent at depth during the spring, summer, autumn, and winter during the A) day and B) night for fish tagged in the Coral Sea between October 2003 and September 2003, after Gunn and Hampton (2003).

The density per unit volume at a depth z, $A_{vol}(z)$, can be expressed in terms of the proportion of the time fish spend at each depth, pf(z), which can be estimated from archival tag data:

$$A_{vol}(z) = A_{sp} * pf(z)\, dz \quad (3)$$

The catch rate for fishing effort is expected to be a function of the vertical distribution of fish, pf(z); the total number of hooks, N; and the vertical distribution of hooks ph(z). Assuming no other factors contribute to the likelihood of a fish taking the bait and being caught, thus the total catch in terms of the spatial abundance would be given by:

$$\text{Catch} = N * A_{sp} * cc * \Sigma\, (\, ph(z) * pf(z) * dz \quad (4)$$

$$\text{Catch Rate (Catch/}N\text{) or CPUE} = A_{sp} * cc * \Sigma\, (\, ph(z) * pf(z) * dz\,) \quad (5)$$

The ratio between the catch rate and the abundance per unit area is termed the catchability and is a function of the sum through the confinement depth, D_c, of the product of the fish density and the hook density.

$$\text{Catchability} = \text{Catch Rate}/A_{sp} = cc * \Sigma\, (\, ph(z) * pf(z) * dz\,) \quad (6)$$

The catchability term is analogous to what is often termed gear performance, which encompasses the vertical distribution of hooks relative to the fish, and the catchability factor, cc, which represents the probability of catching a fish when unit densities of hooks and fish are colocated in a volume. The cc would be expected to be a function of bait, species type, gear performance, and perhaps prey density. For this basic consideration we have assumed that this is approximately constant.

We use the above formulation to estimate the expected proportional changes in catch rate from typical seasonal changes in the vertical distribution of fish to test our initial assumption that spatial changes in catch rate (and abundance) are larger than those expected from changes in the vertical distribution of fish.

The vertical distribution of hooks is known to be a function of gear configuration or HBF (Bigelow *et al*., 2002). Shallow conventional sets (5–6 hooks between floats) fish to a depth range of approximately 90–150 m (~30% 0–100 m, ~70% 100–200 m) and deep sets (> 10 HBF) fish to 100–350 m (~10% 0–100 m and ~30–70%, 100–200 m and ~20–50% 200–300 m, and ~5–10% 330–400 m). In this analysis, we simply assume a vertical hook distribution for 16 HBF (which is representative of the Hawaii-based longline observations filtered by > 10 HBF). Vertical distributions of fish can be estimated from archival tag (PAT/PSAT) observations (Hampton and Gunn, 1998). For qualitative comparison we chose the four seasonal depth distributions of fish from archival tag data in the Coral Sea (Gunn and Hampton, 2003). The tag observations (Figure 1) indicate a seasonal change on the proportion of time spent in the upper water column (f(z)), with a maximum in winter and spring when the waters would be expected to be coolest.

The estimated seasonal change in pf(z) and ph(z) can be used to estimate changes in the catchability at different depths (using equation 6). Assuming a constant cc using our assumed hook distribution, the total catchability seasonal variations are relatively small

(± 15%). As will be presented in Section 4, seasonal spatial variations in catch rate are a factor of more than two (i.e., > 100%). Hence, this first order analysis supports our key assumption that observed seasonal variations in spatial abundance (which we shall see vary by factors of more than three) are larger than expected seasonal variations in catchability. However, it should be noted that this analysis ignores any effect of horizontal or vertical current shear on the vertical distribution of hooks (i.e., gear performance) or seasonal changes in foraging behavior (which could result in variations in the catchability factor).

3.3 The Oceanography of the Hawaii-based Longline Fishery Grounds

The Hawaii-based longline fishery covers the region between the subtropics to 35°N and the equator (0°N) and between 150 and 170°W. Initially we consider the regional oceanography by presenting a latitude-depth section along 170°W of temperature, density, east-west geostrophic current, oxygen and chlorophyll between 0 and 40°N (Figure 2).

In equatorial waters, between the equator and ~4°N, the westward SEC is observed. At the equator the SEC flows above the eastward flowing Equatorial Under Current, EUC (between ~2°S and ~2°N). In this equatorial region, both the currents and the pycnocline depths vary strongly with the ENSO cycle, and the seasonal cycle is relatively weak. The mean thermocline depth is around ~200 m. North of ~4°N, the eastward flowing NECC is observed and the pycnocline shoals to around 100 m at ~8°N. From ~8°N, the NEC flows west, and the pycnocline depth deepens to a maximum of around 250 m at around 18°N. At 170°W, the region north of 18°N is strongly influenced by the Hawaiian Islands, although generally the pycnocline shoals towards 35°N.

Flows in the Hawaiian Islands region are complex. To the east of the islands, the surface flow (as a result of the NEC) is westward but it has maximum flows to the south of the islands between 10°N and 20°N. Flows extend to around 200 m depth, with mean current speeds varying between 0.15 and 0.20 m/s. At the islands, the NEC bifurcates and flows north along the Hawaiian Ridge as the North Hawaiian Ridge Current, NHRC, (Qiu et al., 1997; Firing et al., 1999), and west as the NEC to the south of the Hawaiian Islands.

To the west of the islands, the Hawaiian Lee (and Hawaiian Lee Countercurrent) region extends thousands of kilometers west (Xie et al., 2001). This is a shallow (~100 m) recirculatory region whose flow is driven by spatial variations in wind curl (Chavanne et al., 2002) that result from interaction between trade winds and the topography of the main Hawaiian Islands. This recirculatory region has been documented by drifter observations (Lumpkin and Flament, 2001). Its spatial and seasonal variation has also been considered using velocity sections derived from observations of internal density variations assuming geostrophic balance (Kobashi and Kawamura, 2002). A region of eastward flow, termed the Hawaiian Lee Countercurrent (HLCC), exists close to 20–21°N and varies seasonally in both latitudinal extent and strength (with a maximum of ~0.10 m/s in the fourth quarter). To the north of the HLCC, a region of weak westward flow (~0.05 m/s) between 23 and 25°N (Kobashi and Kawamura, 2002) is bounded to the north by eastward flow in the intermittent Sub Tropical Countercurrent (STC) (Firing and Brainard, 2006). To the south of the HLCC, the NEC flows west.

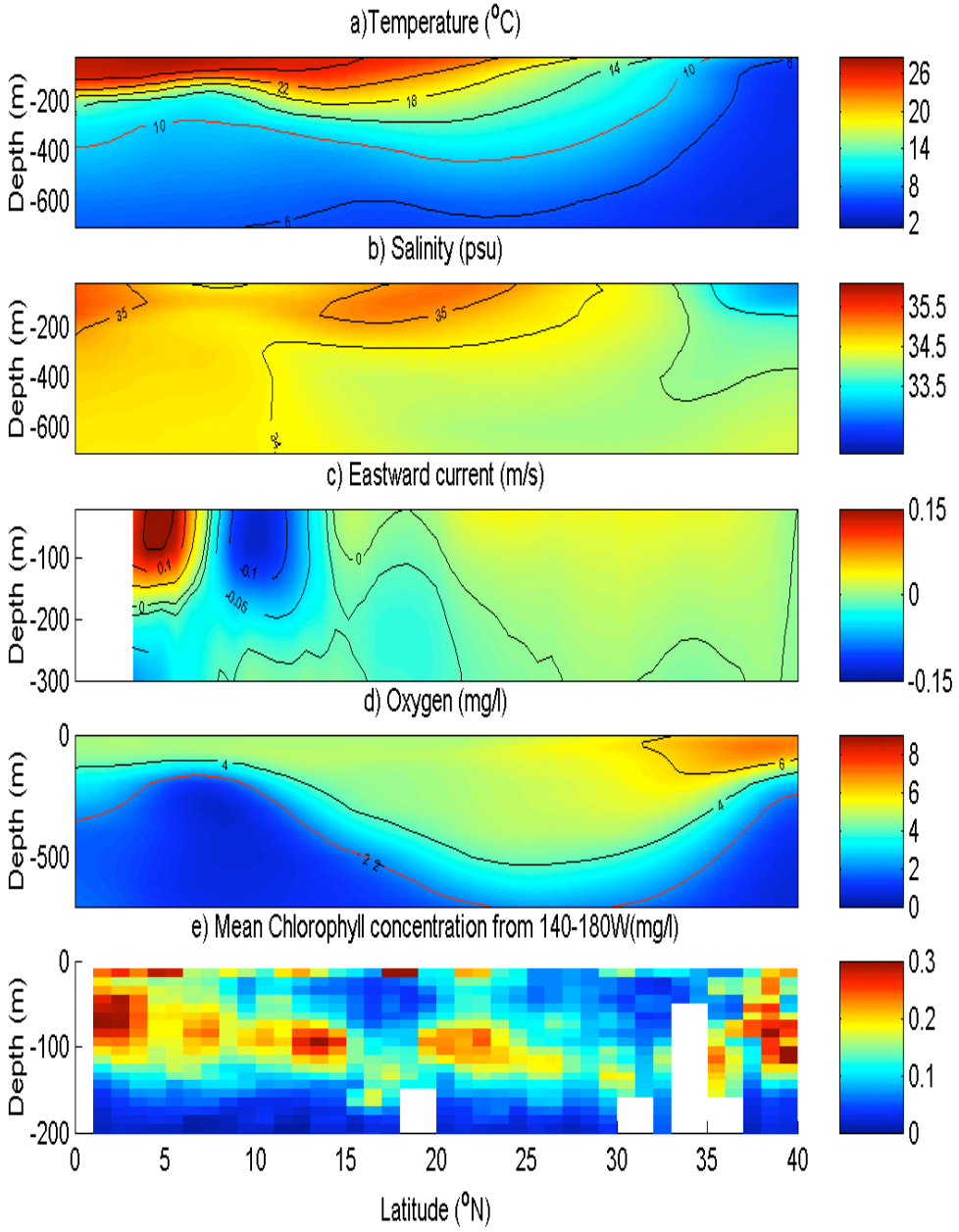

Figure 2. Depth-latitude sections of annual mean temperature, salinity, eastward geostrophic current, oxygen and chlorophyll along 190°E (170°W). With the exception of chlorophyll, all data are gridded observation data from NODC WOA 2001 mean climatology. Chlorophyll data are averages over the 140–180°W longitude band (since data are spars), using all available profile observations from the NODC in 2003. The 10°C and 2 mg/l isolines are plotted as red lines on temperature and oxygen sections, respectively.

The Hawaiian Lee region is also characterized by intense mesoscale eddy activity with eddy kinetic energies more than five times those in surrounding waters (Flament et al., 1997; Patzert, 1969). Vorticity generated by wind shear and the effects of topography and bathymetry close to the main Hawaiian Islands (Chavanne et al., 2003) sets off a train of normally alternate cyclonic and anticyclonic eddies that tend to propagate west to the north and south of 19.5°N, respectively, although they frequently overlap in latitudinal extent. This appears to be most regular over summer periods when eddy kinetic energies are also at a maximum to the west of the dateline (Qiu, 1999). There also appears to be a region of intense eddy activity close to the Cross, Brigham, Swordfish, Bishop, and Daly Seamount group. During fall and winter, smaller intense cyclonic eddies of high productivity intermittently form (Seki et al., 2001). An interesting feature of this region is the division of the lee region into regions to the north of 20°N where cyclonic eddies predominate and a region to the south of 19°N where anticyclonic eddies predominate apparently sustained by wind curl gradients (Lumpkin and Flament, 2001). Anticyclonic eddies are known to propagate as far west as Wake Atoll (Holland and Mitchum, 2001; Mitchum, 1995). Observations of eddy activity at a mooring location and from satellite and model-derived parameters in the Hawaiian Lee are presented in Appendix 1.

In the region between 18°N and 31°N, the seasonal cycle is most pronounced with large annual temperature variations, particularly in the northern region where the annual surface temperature range can be in excess of ~10°C. In this region, significant seasonal north-south migrations of the surface isotherms occur (Figure 3). It is also in this region to the north of Hawaii that a frontal region termed the subtropical frontal zone is associated with high levels of productivity in late summer (Wilson, 2003; Roden, 1991; Bograd et al., 2004).

Figure 3 presents the depths of the 8, 13, 22, and 26°C isotherms from simulations by the JPL ECCO model at 160°W for the upper 600 m of the water column. Significant seasonal temperature variations are evident in the upper 100 m of the water column. At the surface, the region bounding the bigeye preferred upper water (between dive) thermal range of 22–26°C has its maximum and minimum northward extenders in the third and first quarter, respectively. The vertical extent of 22–26°C waters is at a minimum between 8°N and 12°N. Although there are considerable east-west variations in water temperature in the Pacific, the surface seasonal temperature cycle is broadly similar throughout the North Pacific. In the Hawaii-based longline region, the 2.0 g/l oxygen level is shallowest around 5°N (Figure 2), varying between ~100 and 200 m between 0 and 12°N, and deepening north of this region to a maximum of ~500 m at around 30°N.

Acoustic volume backscatter, Sv, has been used as a proxy for densities of crustacean and small fish (Ressler, 2002). Volume backscatter can be estimated from echo amplitude observations from ship and mooring-mounted Acoustic Doppler Current Profilers (ADCPs) (RDI, 1998). There is a large historical database of such observations. RD instruments, 150 kHz and 75 kHz ADCPs, provide estimates of backscatter to ranges of ~300 m and ~600 m, respectively. The variation in volume backscatter through depth with time and latitude from a cruise in the northwestern Pacific (Appendix 1, Figure A1) clearly indicates the diurnal migration of scatterers in the western Pacific and provides an estimate of the depth of the daytime scattering layer. Averaging daytime data could therefore provide estimates of the depth of the scattering layer. Maximum reflectivity

might be expected for scatterers (e.g., swim bladders) of a similar size to the wavelength which for the 75 kHz instrument is 2 cm. Since the scattering efficiency varies with the type of scatterer or organism, it is not currently possible to determine the scatter concentration or type from these observations. In the future, through multi-frequency techniques acoustic methods may become useful in estimating the concentration and type of organisms in the upper ocean and hence provide estimates of the distribution pelagic fish prey.

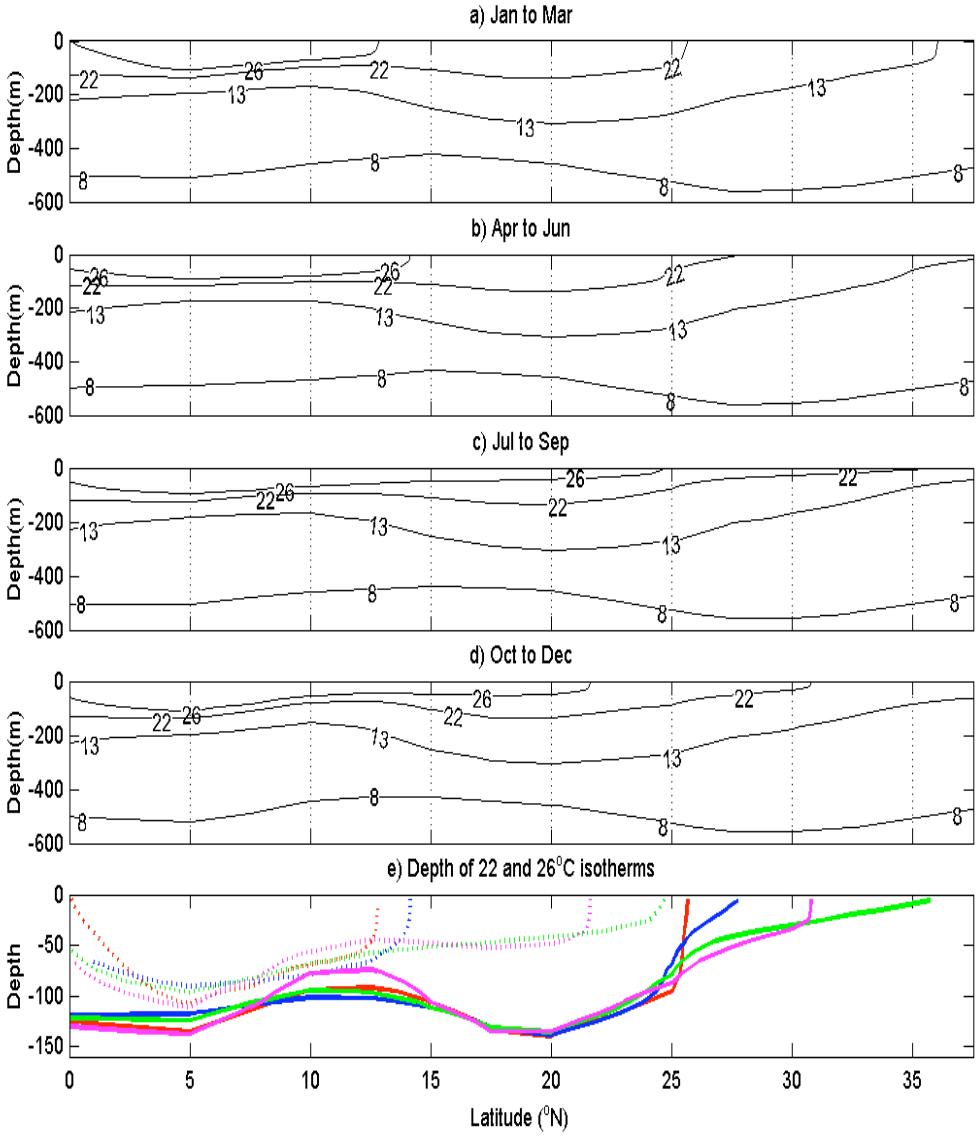

Figure 3. Seasonal variations in depth of the 8, 13, 22 and 26°C isotherms for sections along 161.5°W from the JPL ECCO model analysis. Averaging is over the period 1993 to 2002 inclusive. The lower figure (e) indicates the depth of the 22°C and 26°C isotherms that are indicative of the suggested preferred upper layer temperature for bigeye from tag observations for Jan to Mar (red), Apr to Jun (blue), Jul to Sep (green) and Oct to Dec (magenta).

4. RESULTS OF CATCH RATE ANALYSES

In this section, we discuss spatial variations in catch rate, large scale and seasonal variations in catch rate, the catch rate centre of mass analysis both for the Hawaiian and wider Pacific regions, an interpretation of tag data; and a limited analysis of catch rate data for other pelagic species in the Pacific.

4.1 Spatial Variations in Catch Rate

Catch rates for the Hawaii-based longline fishery averaged over the 12-yr period are presented in Figure 4. Mean catch rate over the whole fishery for the data period showed between 4 and 5 fish per 1000 hooks. Catch rates varied spatially relatively continuously over the region where effort was year-round. There appear to have been variations in catch rate on the scales of ocean variability. A notable reduction occurred in both effort and catch rate in the region between the main Hawaiian Islands and Palmyra waters close to 8–10°N. This was coincidental with the area of expected high shear between the eastward flow of the NECC and the western flow of the NEC; however, it is also a region of elevated thermocline and oxycline. It is also evident from thermal sections (Figure 3) that in this region the preferred thermal range of 22 to 26°C was rather narrow in its vertical extent.

Pronounced variations occurred in catch rate within the Hawaiian Lee region. Both high mean catch rate and the locations of very high catches (> 20 fish per 1000 hooks) were arranged in lines extending northwest parallel to the ridge about 200 km southwest of the ridge and extending to the west southwest from the seamount region close to the Big Island (Figure 4, Appendix Figures A6–A33). There was a region of relatively low catch rate between these regions. These high catch rate regions correspond closely both with the predominant paths of cyclonic (Seki et al., 2001) and anticyclonic (Holland and Mitchum, 2001) eddies that propagate away from their generation region close to Cross Seamount. On average, lower catch rates (and absence of individual very high catches) in this region appear to have been coincident with a region of low mean surface chlorophyll in the fourth and first quarters of the year (Appendix 1, Figure A12), elevated mean sea surface height, i.e., deeper thermocline, (Appendix 1, Figure A6) and negative mean current and wind vorticity (Appendix 1, Figures A19 and A21). Also, high catch regions ran parallel to the islands immediately to the north of the islands in the region of the NHRC, close to the subtropical convergence front to the northeast of Hawaii and in waters close to Palmyra (5°N).

Spatial patterns of catch rate for the six bimonthly periods of the annual cycle averaged over the data period are presented in Figure 5. These highlight seasonal motion of the region of high catch rates which was centered close to the Hawaiian Islands between November and February, moved south towards equatorial waters during the period of March to June, and then moved abruptly north to the waters north of the Hawaiian Islands between July and October.

To inspect catch rate variations and their association with environmental parameters, in more detail we examined weekly sequences of satellite derived parameters such as sea surface temperature (SST), surface chlorophyll *a* concentration, and sea surface height (and derived parameters such as sea surface slope, surface velocity, horizontal shear, and velocity curl).

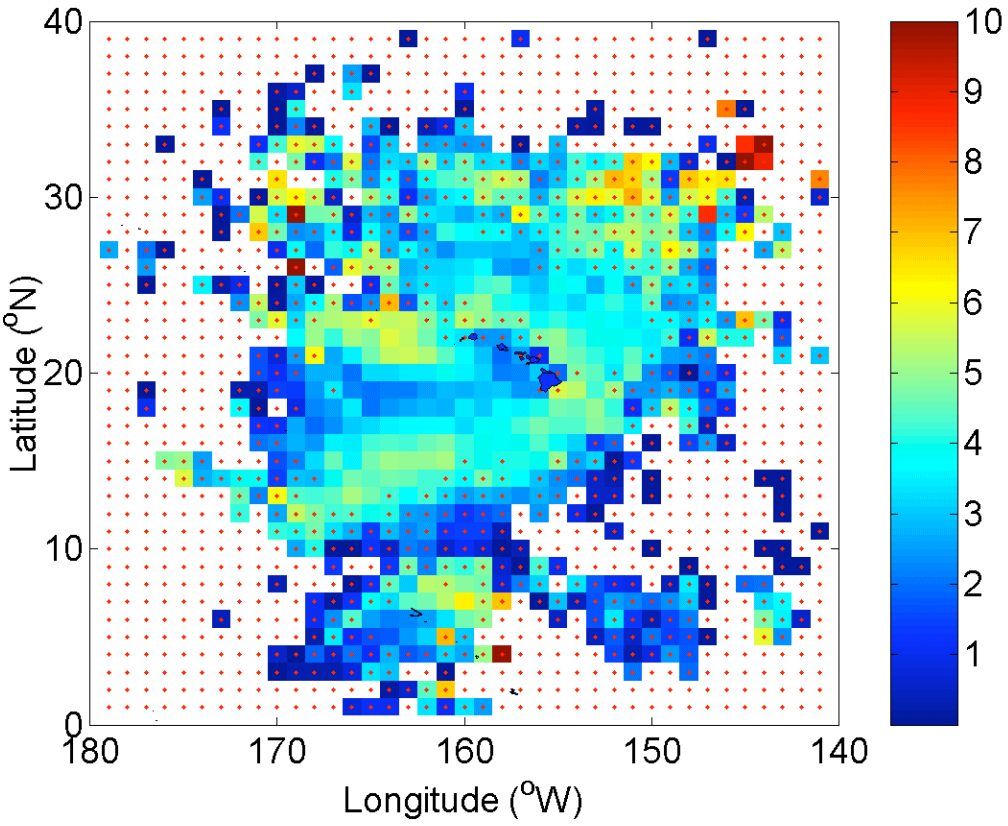

Figure 4. Mean CPUE (or catch rate) for the Hawaii-based longline fishery targeting bigeye over the survey period (1990–2002). Data are averaged in 1° boxes. Red dots denote locations where values may be seasonally biased i.e., there is no effort during one or more of the six bimonthly periods that make up an annual cycle.

It was not possible to identify any clear correlation between catch rates and mesoscale sea surface height anomaly features (i.e., eddy activity) by simple statistical analysis even when focusing on specific regions and periods. It should be noted that the statistical analysis is complicated by the limited number of boats in the Hawaiian fishery, the uneven distribution of effort, and the uncertainty in catch location as a result of the length of the longline. The lack of correlation could also result from masking of the catch rate mesoscale signal by the strong seasonal and interannual variations that are discussed in the next section.

Values of satellite-derived parameters extracted at each of the individual catch rate locations from the Hawaii-based longline fishery are plotted against catch rates in Figure 6. There is a clear correlation between both effort and catch rates and SST with the majority of effort and high catch rates occurring between 22 and 28°C, and maximum catch rates centered on 25°C. Nearly all the high catches occur within this SST range. Some correlation appears to occur between high catches and intermediate values of surface chlorophyll (~0.05–0.10 mg/l). It should be noted that the surface chlorophyll values may be misleading; they do not represent total productivity since the chlorophyll

maxima is frequently located beneath the surface within the thermocline region. Maximum catches appear to have occurred when geostrophic surface currents were at intermediate strength and when vorticity (dv/dx–du/dy) and individual horizontal shear components (du/dy, dv/dx) were close to zero.

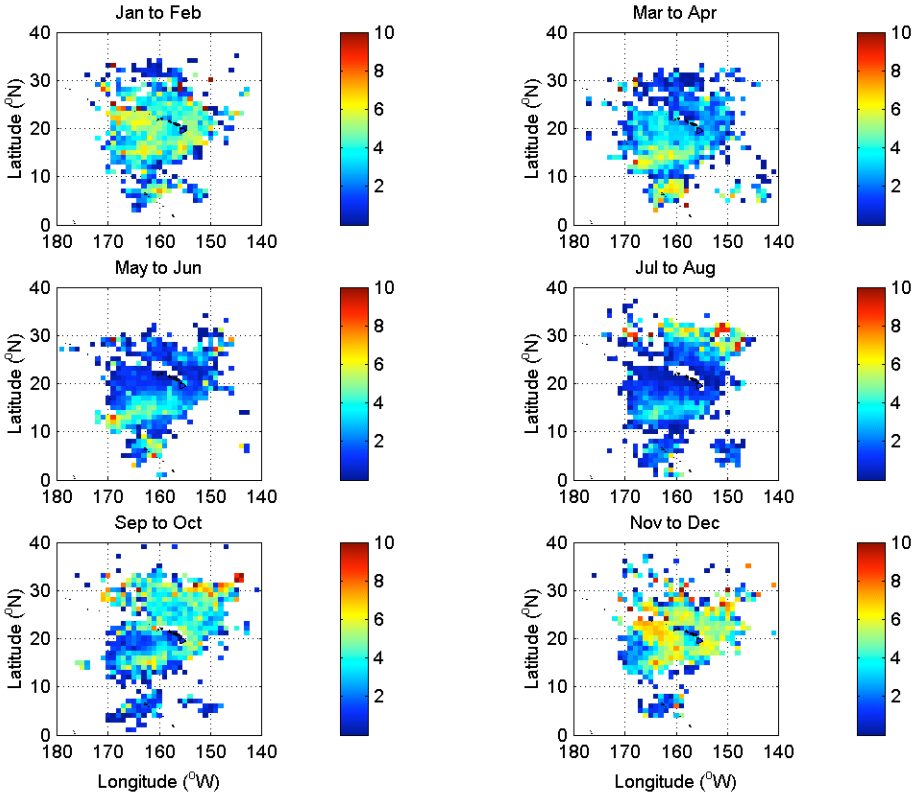

Figure 5. Bimonthly variations in CPUE (or catch rate) distribution over the 12-yr data period (1990–2002).

These results should, however, be treated with caution since vorticity and horizontal shear are second derivatives of sea surface height and are therefore subject to large errors as a result of interpolation of sea surface height between the satellite tracks. These interpolation errors are visible in the spatial comparisons between satellite-derived and model-derived flow parameters and high catch locations which are included in Appendix 1. Geostrophic currents should also by definition be non-divergent (du/dx + dv/dy = 0). This is not evident in Figure 6 providing more evidence of the errors in this analysis. It should also be noted that the geostrophic currents do not include the Ekman currents forced directly by the local wind stress which could also be significant in upper water column (and impact on gear performance).

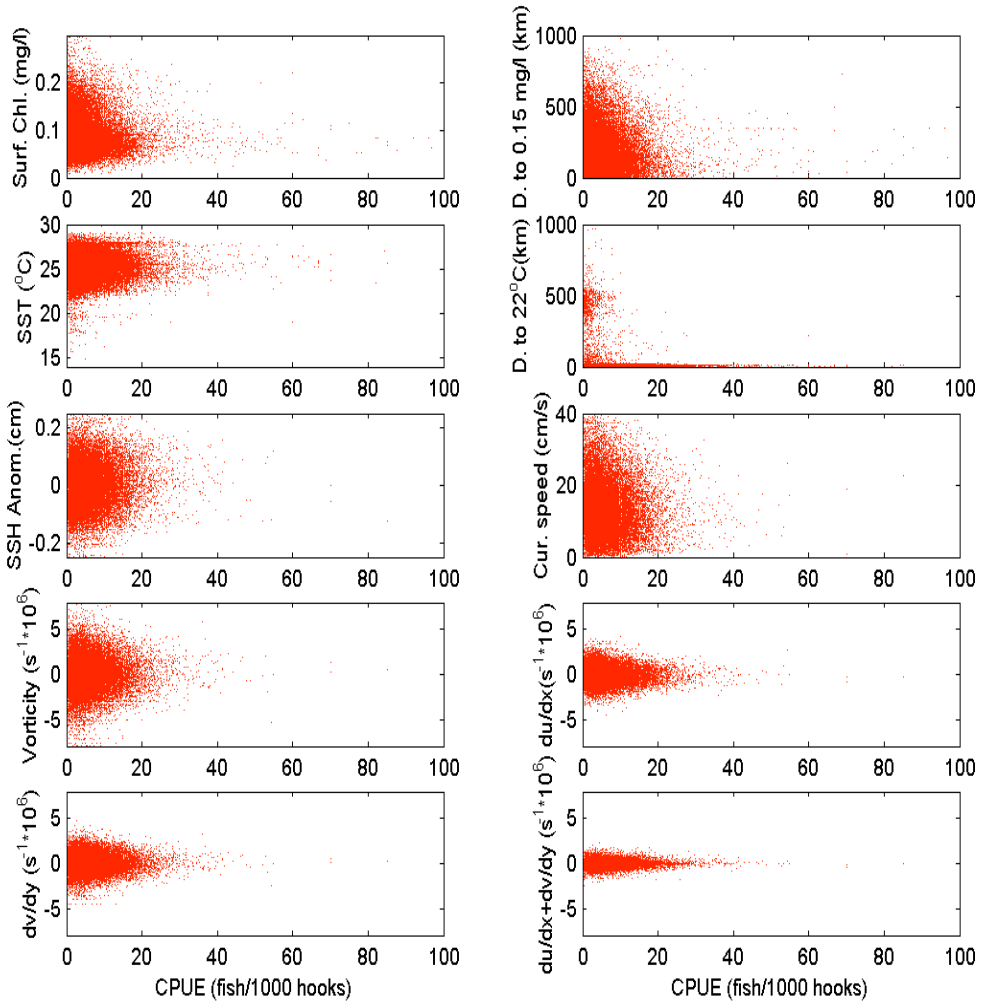

Figure 6. Variation of CPUE (or catch rate) with satellite derived (a) surface chlorophyll *a* (mg/l), (b) distance to 1.5 gm/l chlorophyll contour, (c) sea surface temperature (^{o}C), (d) distance to >22 ^{o}C SST region, (e) sea surface height anomaly, (f) surface geostrophic current speed (cm/s), (g) current vorticity (velocity curl, (h) dv/dx–du/dy), (i) u convergence (du/dx), (j) v convergence (dv/dy), and (k) total convergence (du/dx + dv/dy). All velocities refer to the geostrophic component. Values of second derivatives from gridded data (i.e., convergence and velocity curls) need to be treated with caution. The non-zero values of total convergence that should by definition be zero for geostrophic currents are indicative or errors. Currents do not include the wind forced Ekman transport. Details of satellite data sources and processing are included in Section 2.

However, assuming the comparison between catch rate and satellite-derived shear were valid (i.e., ignoring the errors), the correlation would suggest that low catches correspond to regions of intense convergence or divergence (e.g., associated with paired

eddy activity). This agrees with conventional fishing activity that tends to avoid the regions close to the seamounts where the converging currents tangle the lines. Maximum convergences of ~5×10^{-6} correspond to horizontal motion of 43% of the line length over a 24-hr soak and so might be expected to affect gear performance by altering the distance between floats and, hence, the depth of the hooks. A series of comparisons between high catch locations and a range of satellite and model-derived ocean parameters are included in Appendix 1.

4.2 Large Scale and Seasonal Variations

Interannual and seasonal variations in the bigeye catch, effort and catch rates for the full Hawaii-based longline fishery are presented in Figures 7a and 7b, respectively. There was a general increase in both effort and catch from 1991 until 1998, when catch rate declined sharply. Instantaneous catch rates differed by up to an order of magnitude between summer minima and winter maxima. The mean monthly climatological catch rate (averaged over the 12-yr period) varied between approximately 6.5 and 2.5 fish per 1000 hooks in December and July, respectively.

To inspect catch rates and thermal variations with latitudes, catch and effort were divided into 5-degree latitudinal bands between 10 and 35°N, and a single larger band covering 2.5–10°N for the equatorial region close to Palmyra. Figure 8 presents time series of catch rate and temperature at 10 m and 100 m depth (from JPL ECCO model) for Palmyra at 2.5–10.0°N, the southern Hawaiian Island region at 15–20°N, and the subtropical region at 25–30°N.

In waters near Palmyra (Figure 8, panels A and B), the seasonal temperature variations were relatively small but interannual variations were large. Averaged over the annual cycle there was a seasonal change in catch rate from its maximum when the surface waters were coolest (~28°C) in the first two quarters to a minimum in the last two quarters (although effort was irregular and concentrated in the first two quarters). High catch rates were also correlated with the period during and after upward perturbations to the thermocline, when the temperature at 100-m depth dropped sharply for periods for several months. This was particularly pronounced for the period of early 1998 immediately after a strong upward pycnocline displacement associated with the strong La Niña (during the 1997–98 ENSO period). It should be noted that it appears that the phase of the ENSO cycle and variability are not locked to the annual cycle at this location (i.e., the mean pycnocline depth does not appear to vary significantly seasonally), so the seasonal and ENSO cycles of catch rates are expected to be approximately independent.

In the southern Hawaiian Islands region (15–20°N), (Figure 8, panels C and D), the seasonal thermal cycle was more pronounced. The upper layer remained in the range of 23–27°C through the year and the temperature at 100 m remained fairly stable throughout the year. The bigeye catch rate seasonal cycle was well defined with year-round effort and clear annual cycles with maxima in winter (the fourth quarter), when upper layer temperatures were ~25°C, and minima in summer, typically in June.

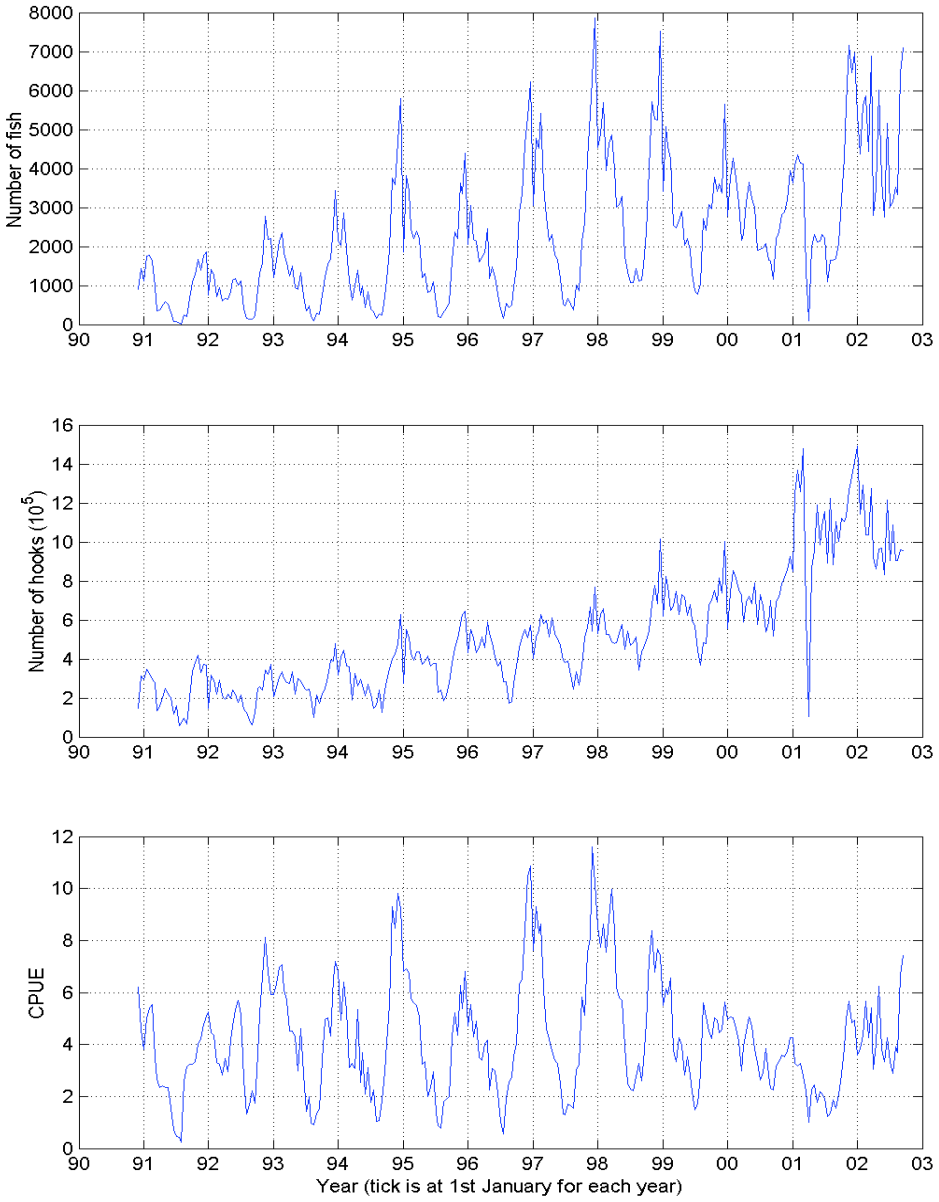

Figure 7. (a) Catch, effort and CPUE (or catch rate) (in 1/24 year sections) for the Hawaii-based longline bigeye fishery from 1990 to 2002.

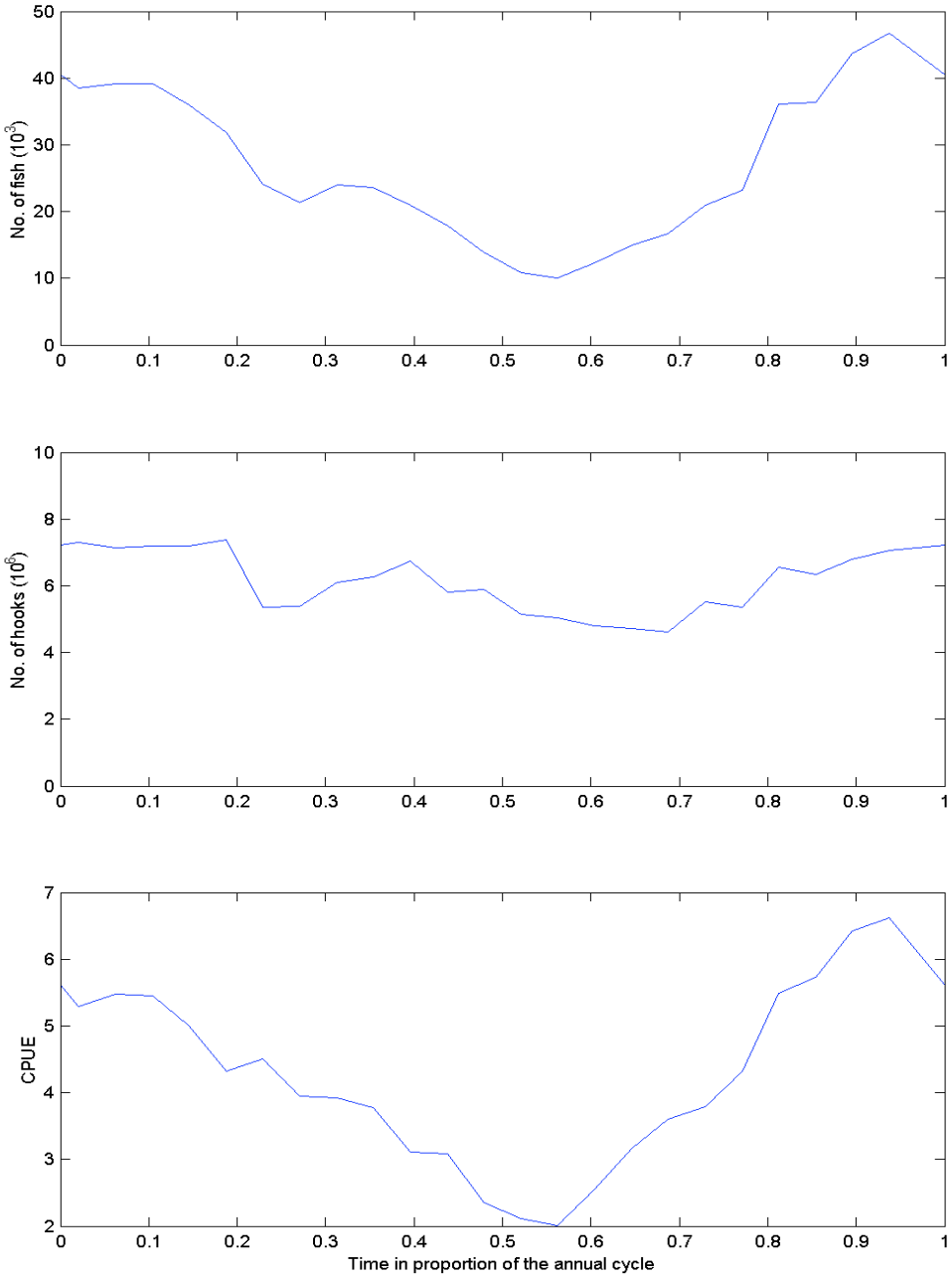

Figure 7. (b) Mean seasonal climatology in catch, effort, and CPUE (or catch rate) for the Hawaii-based longline fishery targeting bigeye tuna over the 12-yr data period.

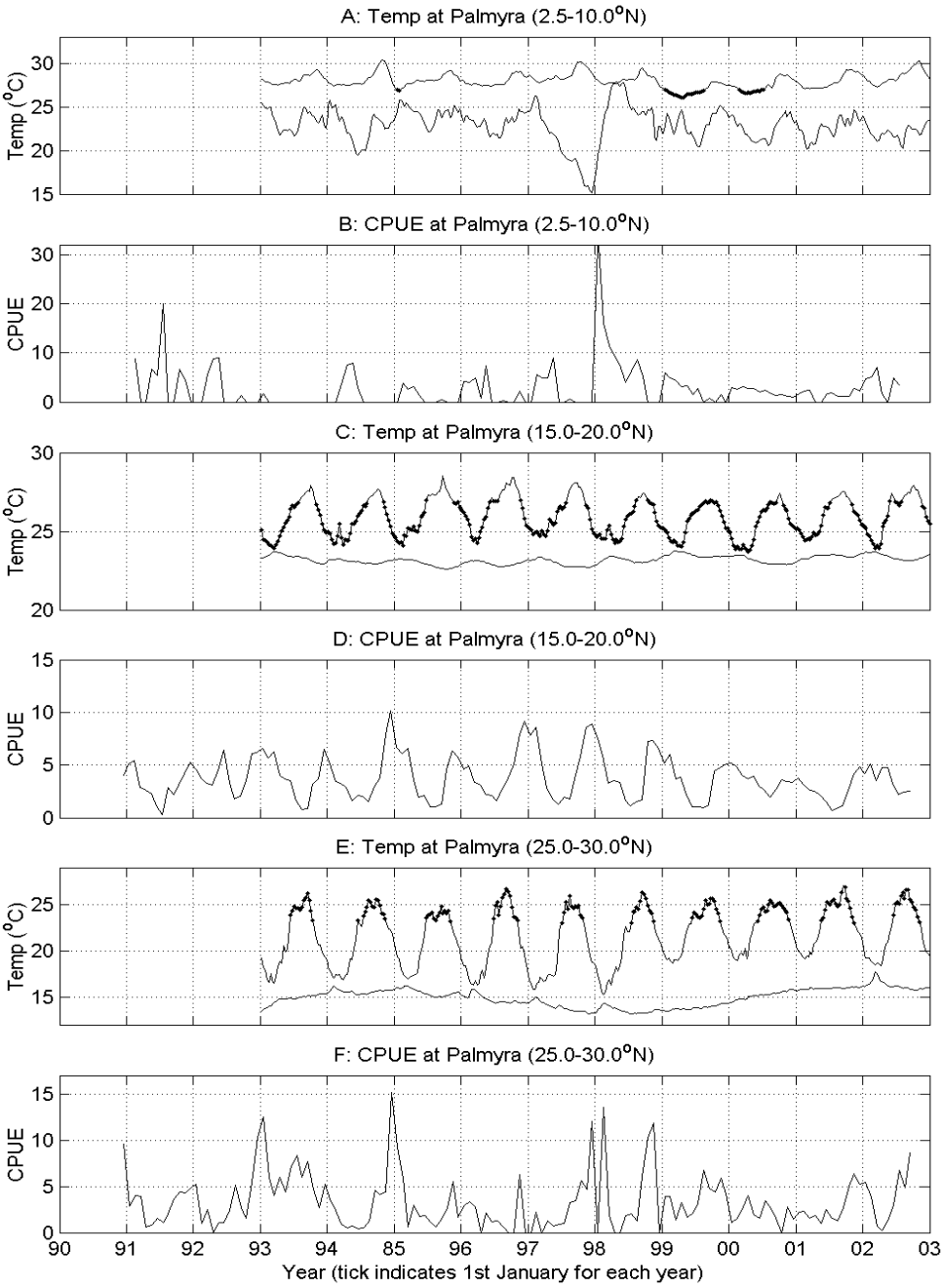

Figure 8. Temperature and CPUE (or catch rate) at 5 m and 100 m depth (from the JPL ECCO model analysis) at latitude of (A and B) Palmyra (2.5–10°N) (C and D) Southern Hawaiian region (15–20°N) and (E and F) Subtropical waters (25–30°N). Surface temperatures between 22°C and 28°C are plotted in bold.

In the subtropical region between 25 and 30°N (Figure 8, panels E and F), the thermal cycle became even more pronounced with annual upper water temperature ranges of up to ~11°C. Significant interannual variations in 100 m temperature appeared to be evident in the JPL ECCO model analysis temperatures in this region. Catch rates were variable, perhaps based on irregular effort, but tended to be maximum in the third quarter when temperatures were highest at ~25°C. The mean seasonal catch rate cycle was continuous with very low catch rates through the first two quarters but maxima in the third quarter with catch rates remaining high into the initial period of the fourth quarter.

Catch rates and surface temperatures averaged over the latitudinal bands in bimonthly blocks are presented in Figure 9. For clarity we do not present error bars which were estimated by calculating the standard deviation of annual variations over each of the 12-yr data period. However, we note that mean catch rates in opposing seasons were significantly different. Catch rate varied relatively continuously despite large variations in effort. There was a noticeable contrast between the bimonthly periods of September to October when the region of maximum catch rate migrated north, and March to April when the region of maximum catch rate was farthest south. This seasonal catch rate migration corresponded to the north-south migration of the region of 22–26°C temperature at 5 m depth. However, the region of high catch rate extended south into surface waters in excess of 26°C. This is perhaps not surprising; in this region, water temperatures within the tag-derived, preferred upper water column, thermal range of bigeye (22–26°C) would have been present deeper in the water column. Relatively low catch rates were observed in the NEC current region close to 10°N in all but the spring period which is consistent with the catch rate spatial analysis presented in Figure 5.

A comparison between mean catch rate and 5 m temperature (from JPL ECCO model analysis) for each latitude and bimonthly block is presented in Figure 10. An apparent preference for surface waters between 22 and 28°C is again evident. This agrees with results derived from both archival tags and our comparison between catch rate and satellite derived SST (Figure 6). This figure also suggests that a small proportion of relatively low catch rates were observed at high latitudes mainly during the first (January–March) and second (April–June) quarters, outside the preferred upper water thermal range.

4.3 COM Analysis and Pacific-wide Comparison

The seasonal average catch, effort, and catch rate latitudinal COM for the Hawaii-based longline fishery are shown in Figure 11. Catch rate COM seasonal variations confirm the migration of the high catch rate region suggested by the spatial catch rate variations (Figure 5). The COM is centered near the Hawaiian Islands around the turn of the year; around 15°N between March and June and around 23°N between September and October. The COM of effort migrates in a similar manner to catch rate but migrates slightly shorter distances since the majority of the effort remains close to the Hawaiian Islands (Figure 9). For the Hawaii-based longline fishery the longitudinal motion is weaker than the latitudinal motion (~60%). It is correlated with the latitudinal COM migration, moving east during northward motion and moving west with southward motion resulting in an overall southwest–northeast annual motion.

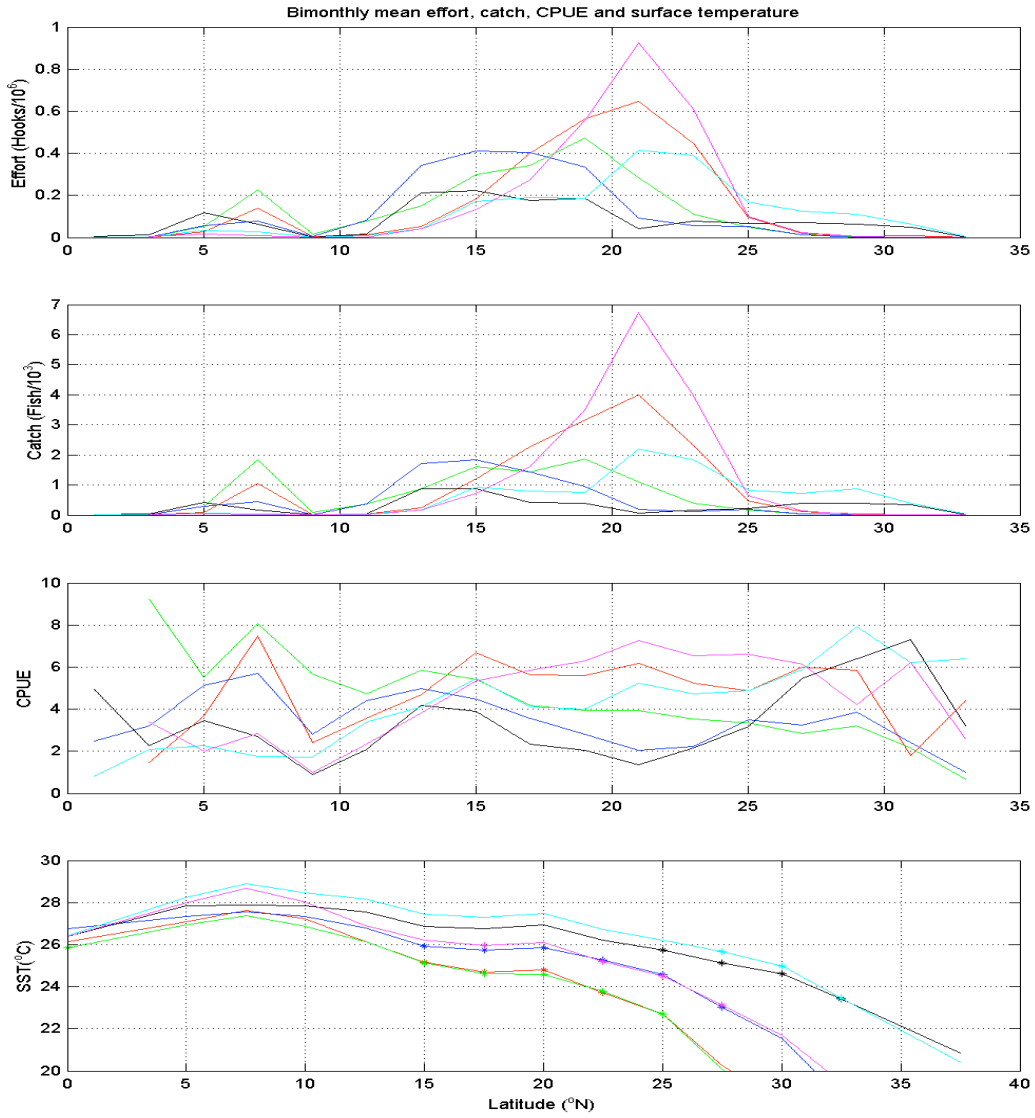

Figure 9. Bimonthly mean effort, catch, CPUE (or catch rate) (from Hawaiian longline fishery data) and surface temperature at 5-m depth (simulated by the JPL ECCO model analysis). The periods are Jan–Feb in red, Mar–Apr in green, May–Jun in blue, Jul–Aug in black, Sep–Oct in cyan, Nov–Dec in magenta. Surface temperature values between 22 and 26°C are marked with *s.

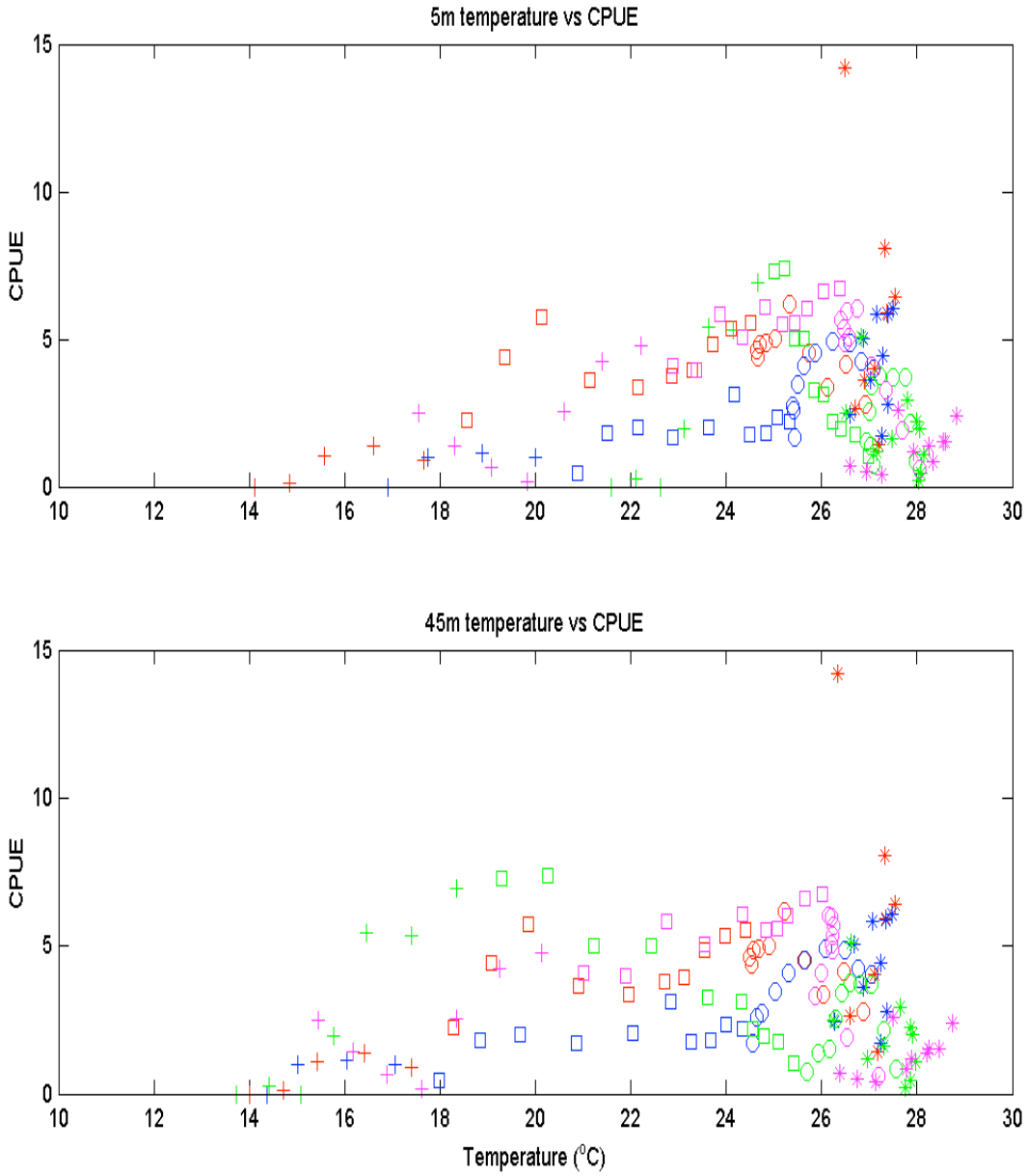

Figure 10. CPUE (or catch rate) versus temperature at 5 m and 45 m (from ECCO model analysis) calculated in latitudinal bands and season. The symbols correspond to latitude bands: 0–10°N (*), 10–20°N (o), 20–30°N (□), 30–40°N (+). The colors refer to seasons: Jan–Mar (Red), Apr–Jun (Green), Jul–Sep (Blue) and Oct–Dec (Magenta).

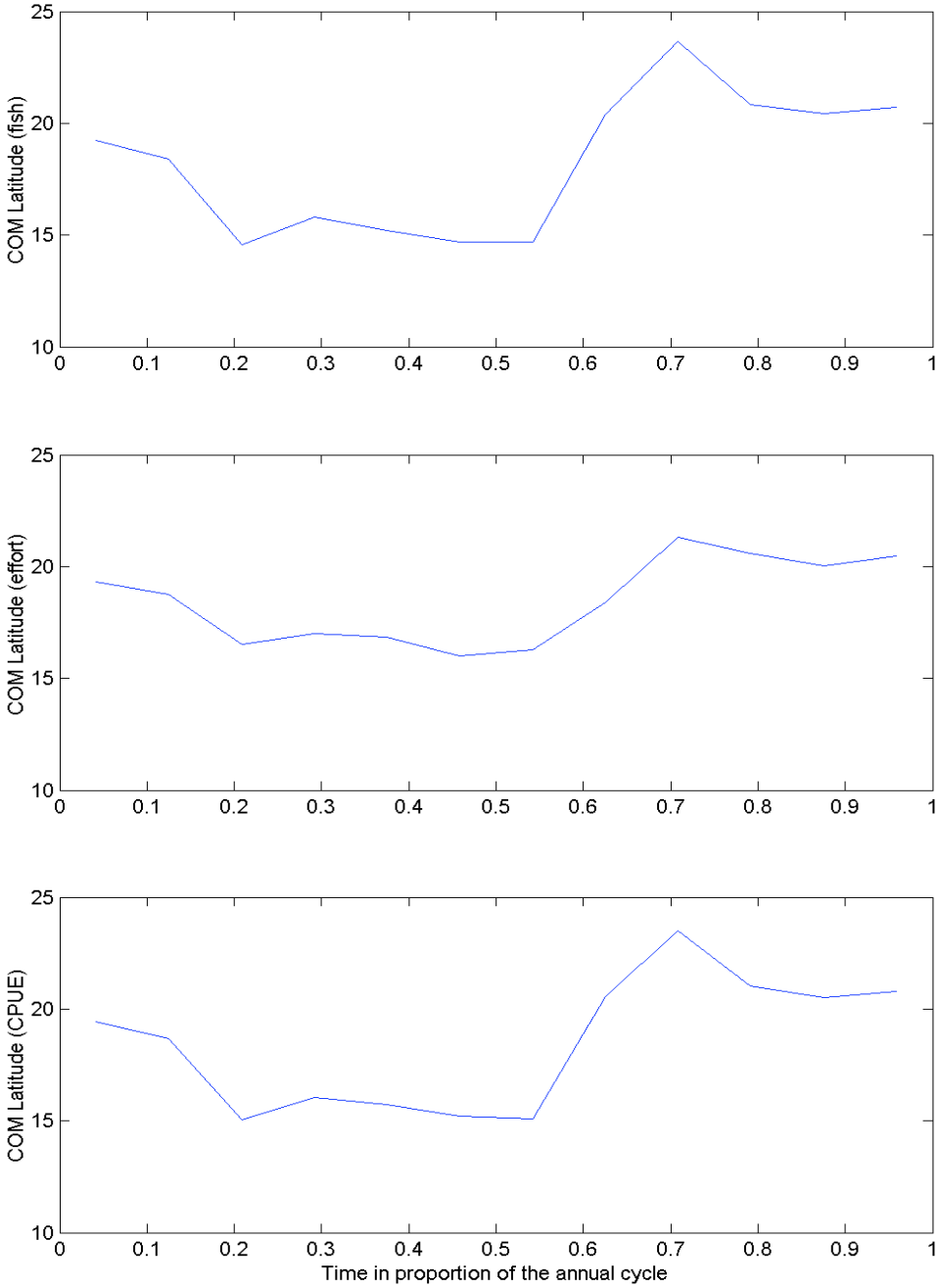

Figure 11. The seasonal variations in the mean catch, effort and CPUE (or catch rate) COM for the Hawaii-based longline fishery targeting bigeye tuna over the data period.

To determine whether the migratory trends in the Hawaii-based longline fishery were also observed for the wider Pacific region, we analyzed Pacific longline data for the Japanese fleet and the SPC all fleets using the region from 160ºE to 130ºW (160–230°E) and 0–40°N, 0–40°S and 40°S–40°N. Land areas and regions without effort within the region may alter the COM motion by biasing the COM through different number of grid cells at different latitudes. For this reason, it is essential that the region used for the analysis has no major land areas and has year-round effort for the seasonal interval chosen. Although the seasons are opposed in the two hemispheres, the seasonal north-south motions of the isotherms are approximately in phase since the poleward direction is also reversed. For some interpretation, we used only the northern hemisphere since effort at all latitudes exceeded a critical threshold for the majority of the year. The southern hemisphere box is presented but may be subject to errors as a result of effort coverage, particularly for the Japanese data. Seasonal catch rate latitude and longitude COM variations can be presented spatially to indicate both north-south and east-west motion. However, this has not been presented as the catch rate migration for bigeye was principally latitudinal.

The catch rate COM migrations for the Hawaii-based Pacific SPC (all fleets) and Pacific Japanese longline data are presented in Figure 12. For Pacific-wide data the mean latitude was removed from the COM variations. Analyses for the northern, southern, and combined hemispheres are presented. The error bars presented are ± 1 standard deviation using annual values for the duration of the data: Hawaii-based (1990–2003), Pacific SPC all fleets (1970–2000), Pacific Japanese (1975–2001). There is good agreement in the catch rate COM variation in the northern hemisphere among all three data sets and a statistically significant seasonal migration. This suggests the annual latitudinal migration of the catch rate COM was Pacific-wide rather than local to the Hawaiian Island region. The catch rate COM variations were approximately in phase with the migration of the surface isotherms in the Hawaiian Lee region (that would be expected to be similar to the Pacific-wide surface isotherm migration). In the southern hemisphere, where fishing effort in the subtropical region was much lower, the migration of the COM was not as well defined as for the northern hemisphere. It should also be noted that averaging both hemispheres removes asymmetries in the annual catch rate cycle.

The bimonthly latitudinal mean catch, effort and catch rates for the SPC all fleet and Japanese Pacific-wide data sets are presented in Figure 13. The catch rate distributions were less regular than the equivalent plots for the Hawaii-based longline but showed broad agreement in overall catch rates for all the data sets. Both Pacific-wide data sets clearly indicated large seasonal variations in the bigeye catch rates in both hemispheres in the subtropical regions (15–40°N/S) and indicated the expected maximum in the subtropical catch rate in the opposite seasonal period in the two hemispheres.

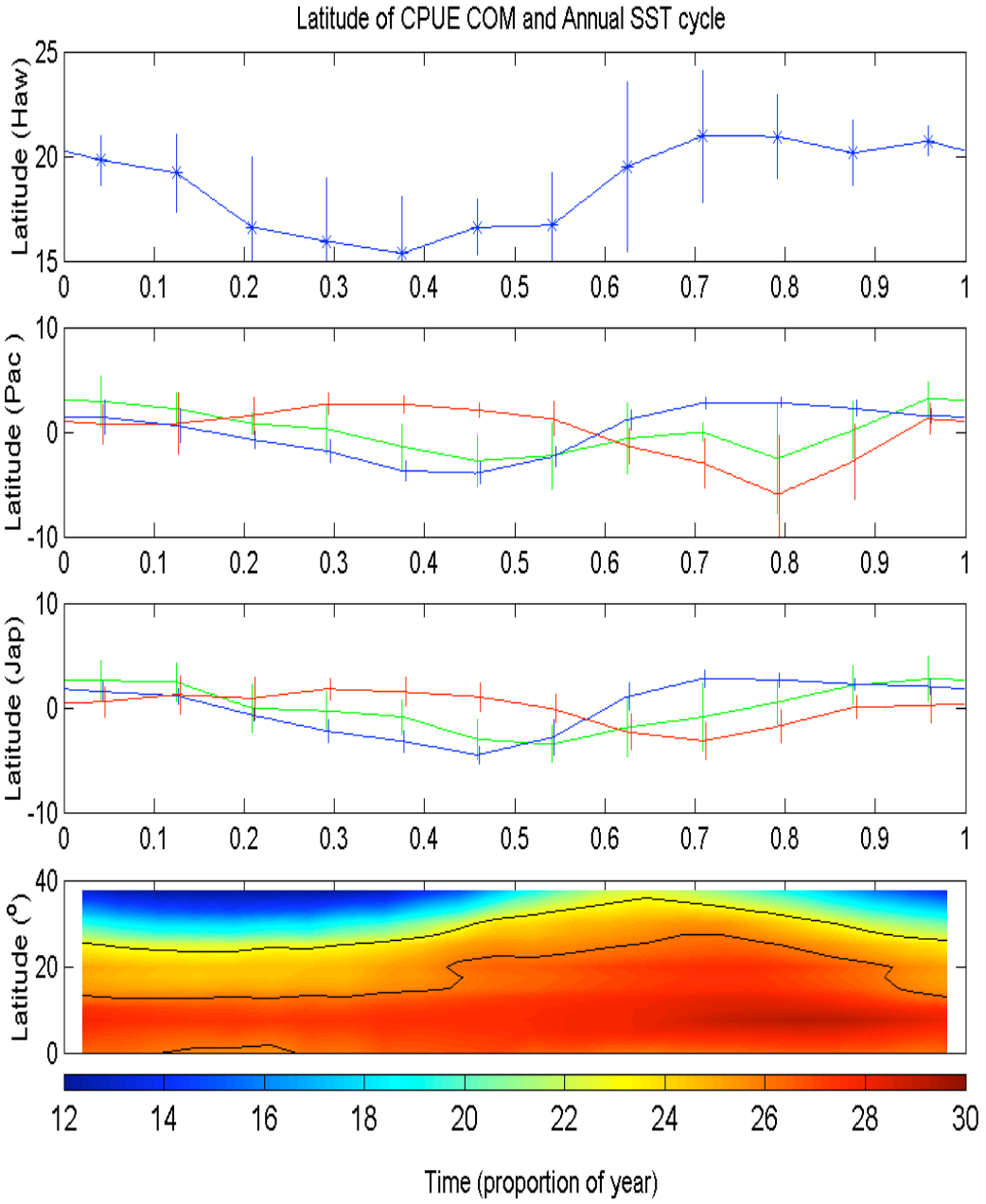

Figure 12. Mean CPUE (or catch rate) COM latitude for the Hawaii-based and the Pacific (SPC all fleet) and Pacific (Japanese) fisheries targeting bigeye tuna. COM latitudes for the Northern hemisphere box are in blue (160–230°E and 0–40°N), for the Southern hemisphere are in red (160–230°E and 0–40°S), and for both hemispheres are in green. The 5 m depth temperature derived from seasonal averages over the data period of the JPL ECCO model analysis (with the 22 and 26°C isotherms marked in black) is presented below.

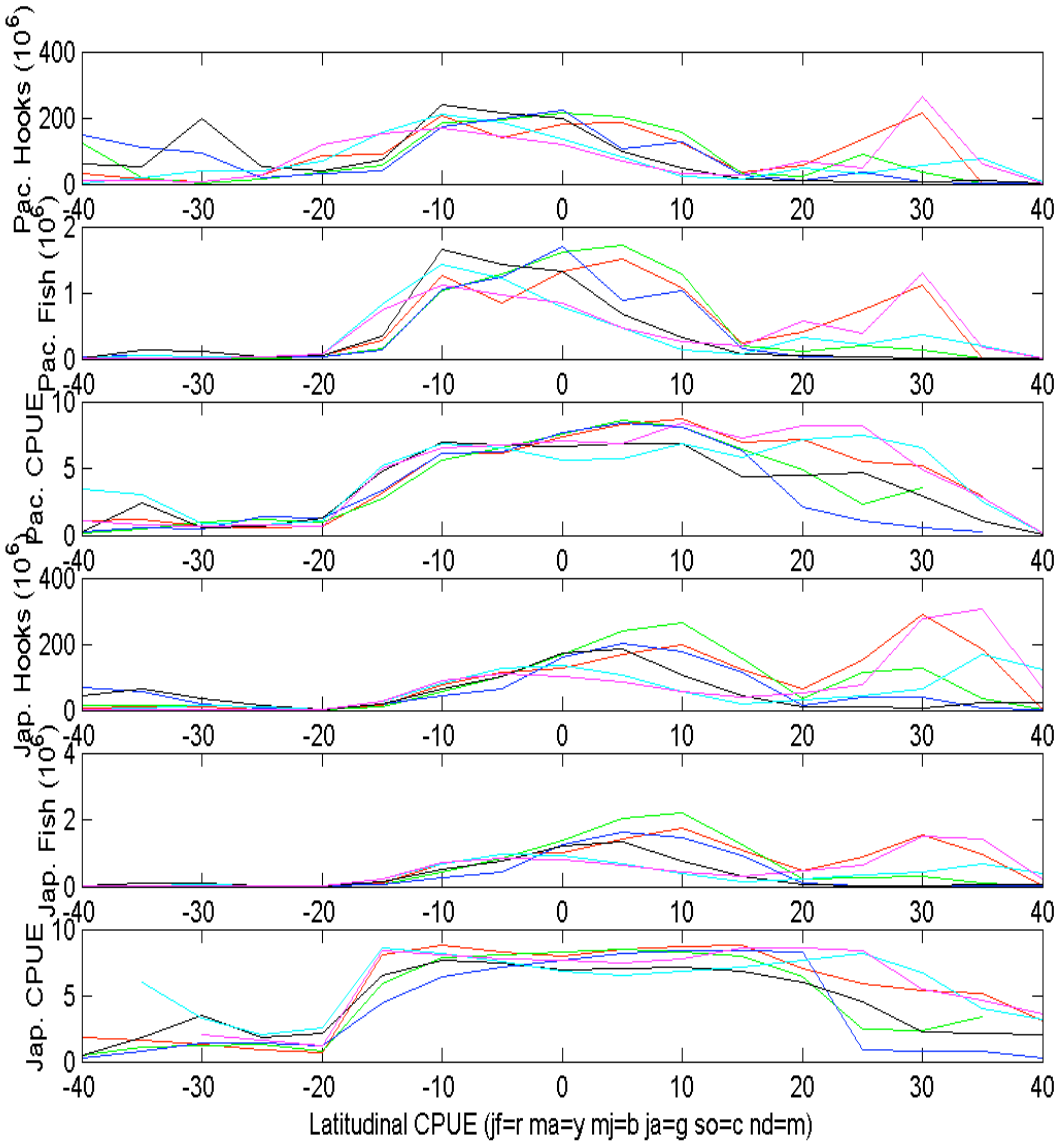

Figure 13. Bimonthly catch, effort and CPUE (or catch rate) across the whole Pacific region for the (a) Japanese and (b) SPC all fleet Pacific longline bigeye fishery. The region used for the analysis is from 40°S to 40°N and 160°E to 230°E for both data sets. Periods are Jan–Feb (red), Mar–Apr (green), May–Jun (blue), Jul–Aug (black), Sep–Oct (cyan) and Nov–Dec (magenta).

For the Central Equatorial Pacific region, including Palmyra (180°W–160°E and 10°S to 10°N) we briefly consider catch rate variations associated with ENSO fluctuation since ENSO is known to impact on tuna populations (Lehodey, 2001; Lehodey, 2000; Lehodey et al., 1997; Howell and Kobayashi, 2006). This region is known to be influenced by ENSO variations, with periods of depressed thermocline during El Niño conditions followed by periods of elevated thermocline during the subsequent La Niña cycle. There is a striking correlation between catch rates and the Multivariate Enso Index, MEI; Southern Oscillation Index, SOI; and the reciprocal of the depth of the 15°C isotherm derived from the SODA data set (Figure 14). A linear correlation between catch rate and isotherm depth would be consistent with the vertical concentration of fish by ENSO-related pycnocline motions. However, a more detailed analysis of the lag between the pycnocline depth and catch rate is required to separate spatial abundance changes associated with ENSO variations (which might be expected to have a time lag relative to the ENSO cycle) from catchability changes due to vertical concentration (which would be expected to be directly correlated with isotherm or oxycline depth with no lag).

4.4 Comparison with Tag Data

To determine whether the observed migration in catch rates relate to the actual migration of fish we inspected tag data from bigeye tuna tagged both at seamounts close to the main Hawaiian Islands (provided by D. Itano) and in the southern Pacific using the CSIRO/SPC Pacific bigeye tag data set (provided by J. Gunn). Data were filtered to include only tagged fish when the release to capture time was more than 1 month and the displacement was greater than 3º in latitude. This represented a small minority of the fish for the Hawaiian Islands tag data set which focused on a seamount group close to the main Hawaiian Islands. For the SPC data, only tags in the region between 8 and 28°S were considered. For both of the two regions, poleward of 15°N/S there appeared to be a tendency for the majority of fish to move north for the second two quarters of the year and south in the first two quarters of the year (Figure 15). However, the migration evident in the tag observations did not appear to occur for as large a proportion of the tagged fish as one might expect from the large seasonal changes in catch rate.

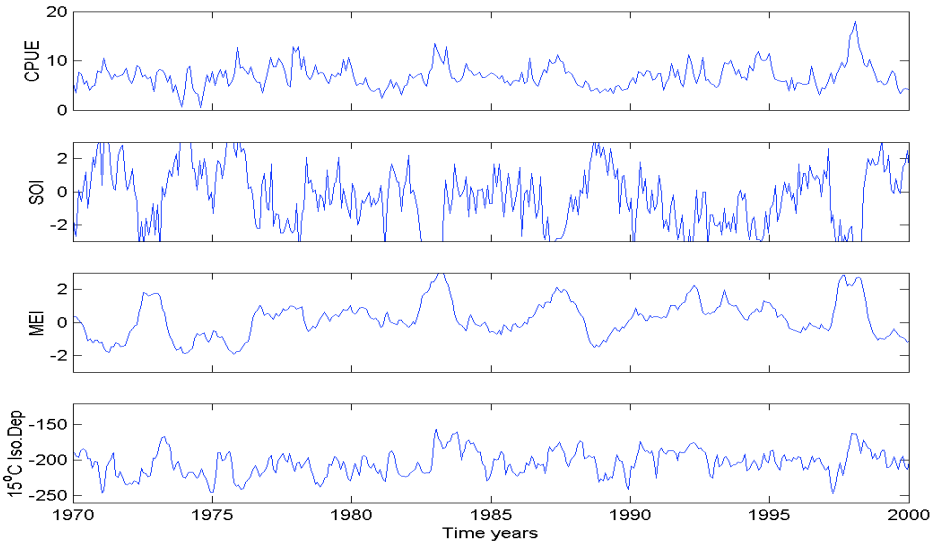

(a)

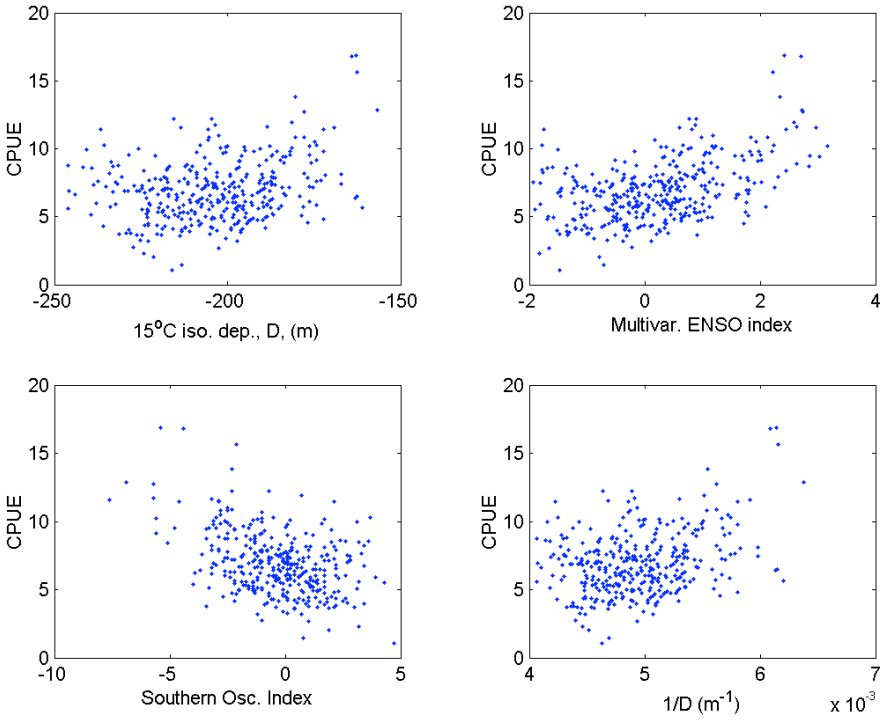

(b)

Figure 14. (a) Temporal variation in CPUE (or catch rate) for bigeye for the Central Equatorial Pacific region (180–200°E 10°S–10°N), the multi-variant ENSO index (MEI), the Southern Oscillation Index (SOI) and the depth of the 15°C isotherm at a central location (200°E 0°N) derived from the SODA analysis. (b) Correlation between CPUE (or catch rate) and the MEI, SOI, isotherm depth and reciprocal of the 15°C isotherm depth.

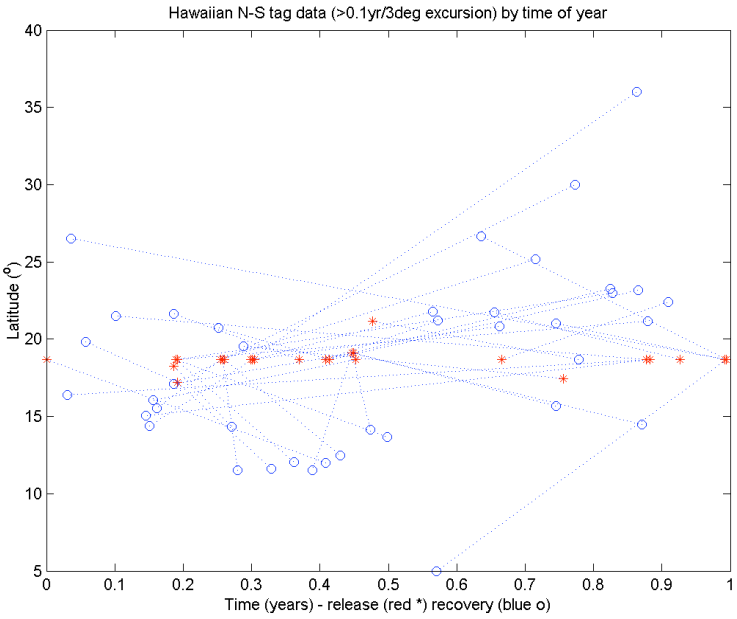

(a)

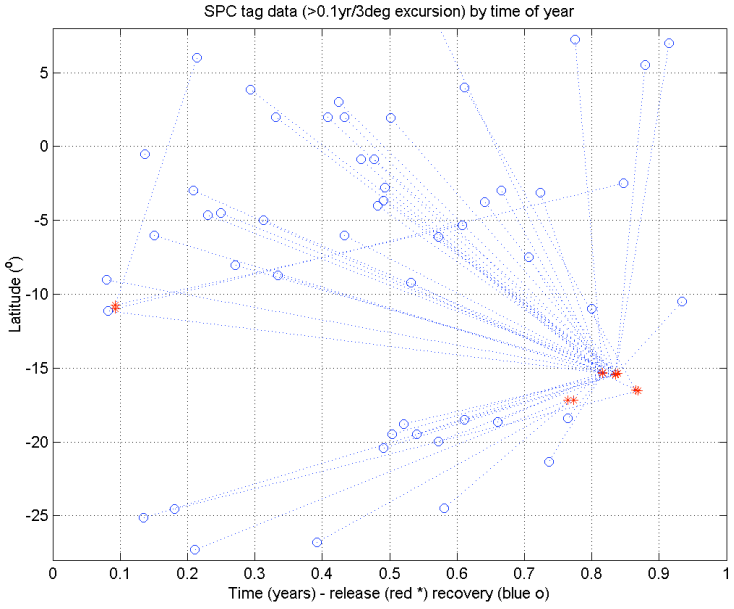

(b)

Figure 15. Seasonal variation in release and retrieval latitudes for tags releases in the (a) northern and (b) southern subtropical (> 15°N/S) Pacific. Red stars represent the release time of year and latitude, whilst the blue circles represent the corresponding capture time of year and latitude. Tag data for the northern hemisphere are provided by Itano and Holland (University of Hawaii) and tag data for Southern hemisphere in Coral Sea are provided by Gunn and Hampton (SPC). Data are filtered to include only tags for bigeye that moved more than 3°N/S and that were captured more than 0.1 year after release.

4.5 Other Pelagic Species

Using the SPC all fleet and Japanese Pacific data we inspected the migratory behavior of albacore, yellowfin tuna, striped, blue and black marlin and swordfish. To investigate catch rate migrations, we considered the latitudinal variation in the catch rate COM for each of the various species in the North Pacific region (160°E−130ºW, 0−40°N). For all species, except swordfish which is a targeted shallow set fishery, there was very close agreement between the species for the Japanese and SPC all fleet data (Figure 16). Bigeye, albacore, and swordfish catch rates appeared to migrate approximately in phase with the annual isotherm motion, whilst striped and blue marlin catch rates appear to have migrated with a significant difference in phase. On average, swordfish, albacore, and striped marlin catch rates were farther north than for the other species. Figure 17 presents the bimonthly latitudinal variation in catch for albacore, yellowfin tuna, bigeye tuna, striped marlin, blue marlin and swordfish for the Japanese Pacific fleet longline catches (fishing effort is as presented in Figure 13). Longitudinal migration is not considered since it is more complex because of large longitudinal variations in effort.

Seasonal variations and correlation between catch rate and ENSO variations for bigeye tuna in the equatorial Pacific region close to Palmyra (180–220°E, 10°S–10°N) were also evident for other pelagic species but this analysis has not been presented.

5. DISCUSSION

Analysis of catch rates from the Hawaii-based and Pacific-wide bigeye tuna longline fisheries has revealed some interesting variations which, if interpreted with care, appear to provide useful insight into the spatial distribution of fish. In particular, catch rates varied over a range of time and length scales from mesoscale to seasonal to interannual, apparently in relation to changes in the ocean environment.

Spatial variations in bigeye tuna catch rate appear to correlate with oceanographic features over the Hawaii-based longline region. In particular, reduced catches in the NECC region occur where the preferred thermal range within the upper layer between dives might be expected to confine the fish vertically and where the preferred bigeye oxygen and thermal ranges are shallowest. The alignment of high catch regions in the Hawaiian Lee to the southwest and northwest of the seamount region could correspond to either the direction of propagation of mesoscale ocean features or the surface transport which floating aggregates might follow. This could be consistent with fish known to be associated with the seamount region (Sibert et al., 2000) becoming associated with features or floating objects as they move or propagate away to the west. However, it should be noted that catch rate variations could also be influenced by high spatial variability in current speed, horizontal current shear, horizontal current convergence, surface chlorophyll, wind characteristics, etc., that are evident in the analysis included in Appendix 1. In particular, there appears to be a tendency for low catches (or the region with no high individual catches) to be coincident with a region of elevated mean sea surface height, i.e., deeper thermocline, low winter mean surface chlorophyll, negative mean current vorticity, and negative mean wind vorticity.

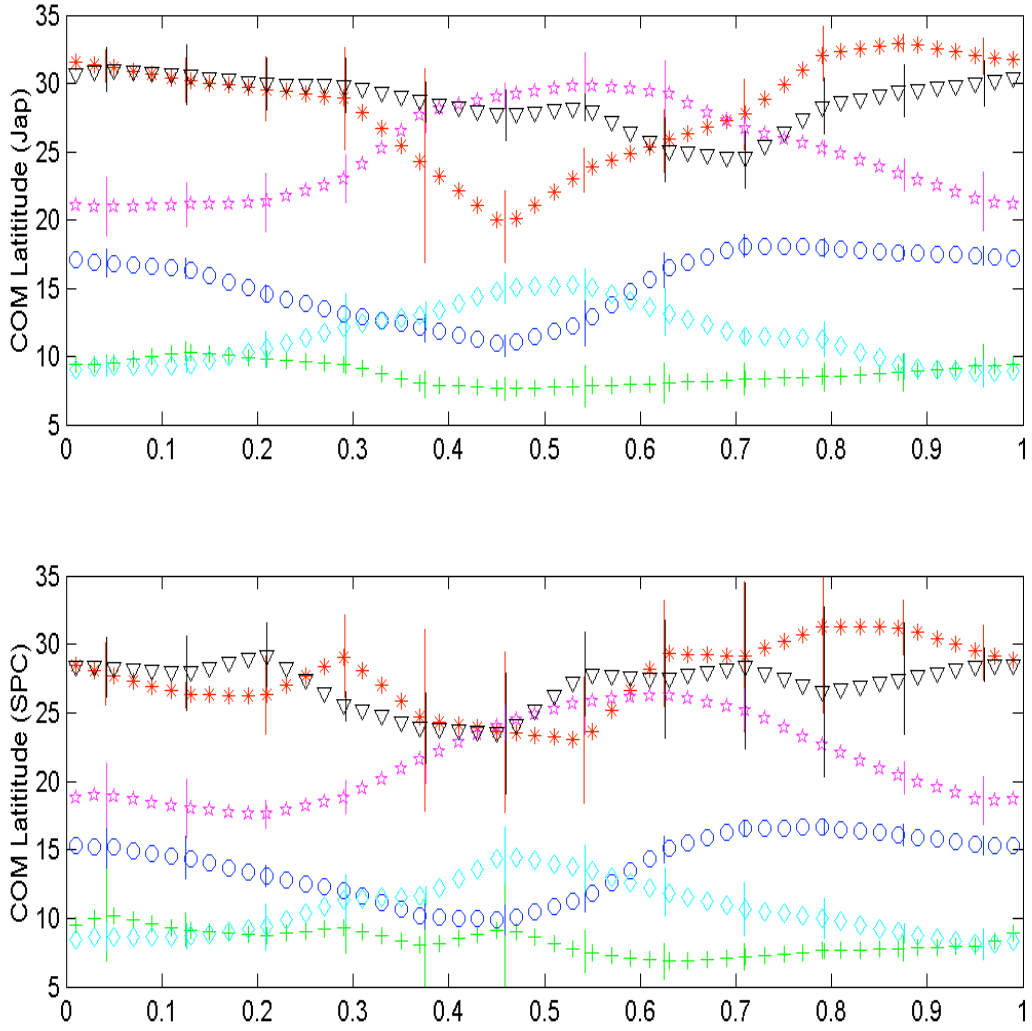

Figure 16. Seasonal variation in the CPUE (or catch rate) COM latitude for various pelagic species for the region (160–230°E 0–40°N) for (a) Japanese Pacific fleet (b) the SPC Pacific all fleet data. Species are albacore (red), yellow tuna (green), bigeye tuna (blue), striped marlin (magenta), blue marlin (cyan), sword fish (black).

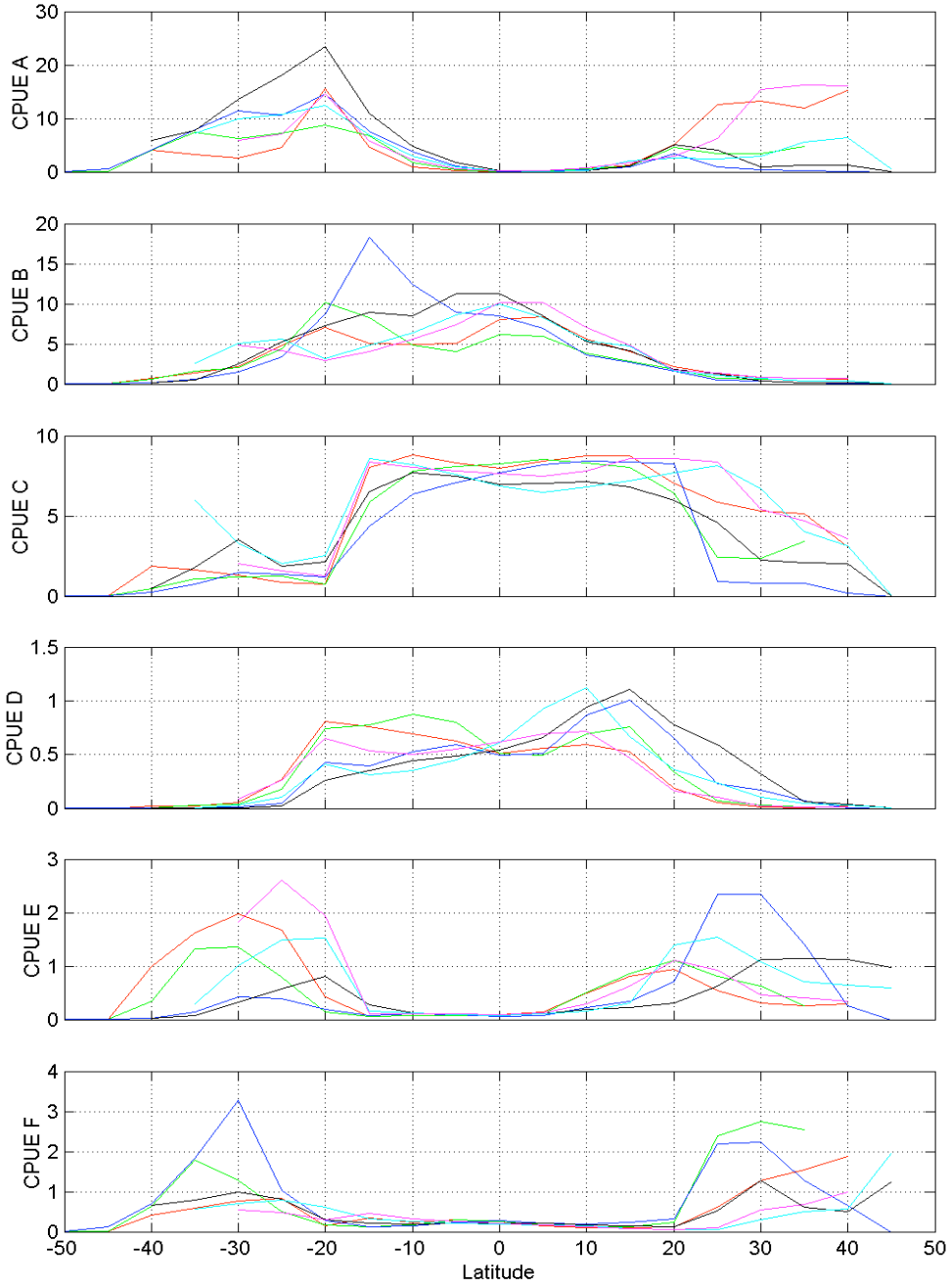

Figure 17. Latitudinal CPUE (or catch rate) variation for the Japanese Pacific longline fishery (55°S to 55°N and 160–230°E) . Note: effort is common for all species. Species are (A) Albacore, (B) Yellowfin Tuna, (C) Bigeye Tuna, (D) Striped Marlin, (E) Blue Marlin and (F) Swordfish. Periods are: Jan–Feb (red), Mar–Apr (green), May–Jun (blue), Jul–Aug (black), Sep–Oct (cyan) and Nov–Dec (magenta).

The Hawaii-based longline catch rate data confirm the known pronounced seasonal catch rate variations for bigeye tuna (presented for various pelagic species for the Hawaiian Islands by Curran *et al*., 1996). Spatial catch rate variations indicate an annual latitudinal migration of the high catch rate region. This high catch rate region was centered close to the Hawaiian Islands between November and February, moved south towards equatorial waters during the period of March to June, and then moved abruptly north to the waters to the north of the Hawaiian Islands between July and October. This seasonal motion is confirmed by a seasonal north-south motion of the catch rate COM. The north-south motion of the catch rate COM approximately follows the north-south seasonal motion of the isotherms of the preferred thermal range, which suggests the migration could be driven by a near surface temperature preference. Correlation between bigeye catch rate and surface temperatures (derived from satellite and the JPL ECCO numerical model) reveal that the high catches tended to occur in water temperatures in the region of 22 to 28°C with maximum catch rates around 25°C. This is consistent with archival tag data which suggest that bigeye tuna have a preferred between-dive or nighttime thermal range of between 22–26°C since when surface temperatures are > 26°C the fish could find the preferred thermal range by locating themselves deeper in the water column. However, the observed migration in catch rate suggests that the inferred southward migrations are farther than would be required solely from the preferred surface temperature range. This could suggest that they are associated with foraging or spawning. The movement of fish to the north of the Hawaiian Islands in late summer is also coincident with a time of high productivity in this region.

Latitudinal catch rate sections and the COM motion for the Hawaii-based longline fishery indicate a threefold seasonal change in catch rate for the Hawaii-based longline fishery with significant differences between opposing seasons. Pacific-wide data for the region 160°E–130°W and 40°S–40°N indicate similar seasonal catch rate changes in the North Pacific in both the Japanese and SPC all fleet data. This annual cycle is not well defined in the southern hemisphere where effort is not year-round. The COM analysis suggests that significant catch rate migrations are observed for several pelagic species including albacore, bigeye, and swordfish which are broadly in phase with the ocean thermal cycle. However, for striped and blue marlin, it appears that migration varies at a different phase to the annual thermal cycle. Tag observations support the inferred migrations for bigeye although the proportion of fish exhibiting the migration is not as high as expected from the seasonal changes in catch rate. It, therefore, appears that the catch rate COM, if employed with care, may be a useful parameter to indicate catch rate migration.

Correlation of catch rate with isotherm variations associated with ENSO variations was evident for bigeye in the central equatorial Pacific (between 180°E–160°W and 10°N–10°S) region close to Palmyra based on the Pacific wide data, which could suggest vertical confinement by isotherm depth perturbations influence catches. However, analyses by Howell and Kobayashi (2006) of bigeye catch rates near Palmyra suggest that the situation may be complex, with horizontal fish motions and currents also playing a significant a role in determining catches. Further work is required to establish whether the observed variations are simply a result of variations in vertical distribution of fish or also a result of horizontal fish movements correlated with ENSO fluctuations.

The seasonal variations in catch rate are consistent with the hypothesis that bigeye have a physiological preference for a specific water temperature range to warm blood and external body tissue between dives. It is possible that outside their preferred near surface temperature range the bigeye dive cycle may be restricted. More tag observations (Sibert *el al.*, 2003) are needed to confirm whether this is the case. Further tag observations are also needed to determine how the migrations of individual fish contribute to the observed migration in catch rate (and to determine how the catch rate changes related to migratory changes in abundance). These data would also facilitate quantitative estimation of the extent to which variations in catchability influence our inferences on seasonal migration. In our simplified analysis, we do not expect this contribution to represent a large proportion of the observed seasonal catch rate variations. This analysis does not include the effects of horizontal and vertical current shear and convergence on gear performance through its impact on the vertical distribution of hooks or tangling lines. However, mean changes in these parameters over the seasonal temporal and spatial scales of our migration results are not expected to be sufficiently large to significantly alter our inferences.

The principal hurdle to making accurate stock estimates is the conversion of observed catch rates into estimates of total abundance per unit area which requires accurate estimates of the vertical distribution of both fish and hooks (and parameter we termed the catchability factor). The vertical distribution of bigeye is known from tag data and is likely to be a function of various environmental parameters including the temperature, oxygen, and prey species abundance (including the depth of the scattering layer). It may, in the future, become possible to estimate prey distribution from acoustic observations of the deep scattering layer. Further work and more tag observations are required to facilitate the use archival tag data to improve estimates of the vertical fish distribution with respect to these environmental parameters. This tag information could also be used as an independent check of inferred migratory behavior from catch rate observations. The hook distribution is a known function of the gear configuration (numbers of hooks between floats). Recent improvements in high resolution assimilative ocean models provide improved estimates of vertical and horizontal variations in currents, including shear, convergence, etc., which are known to effect gear performance and the vertical hook distribution. These models also provide estimates of mesoscale variations in ocean thermal structure (i.e., eddy characteristics). In combination, this information could facilitate the assimilation of catch rate data together with accurate environmental information into future population models to improve stock estimates and our understanding of migratory behavior of pelagic fish.

REFERENCES

Bertrand A, Josse E, Back P, Gros P, and Dagorn L (2002). Hydrological and trophic characteristics of tuna habitat: consequences on tuna distribution and longline catchability. *Can J. Fish. Aquatic Sci*., 59, 1002-1013.

Bigelow K, Hampton J, Miyabe N (2002). Application of a habitat based model to estimate effective longline fishing effort and relative abundance of Pacific bigeye tuna (*Thunnus obesus*). *Fish. Oceanogr*., 11:3, 143-155.

Boggs C H (1992). Depth, capture time and hooked longevity of longline-caught pelagic fish: timing bites of fish with chips. *Fish. Bull. U.S.*, 90, 642-658.

Bograd S J, Foley D G, Schwing F B, Wilson C, Laurs R M, Polovina J J, Howell E A, and Brainard R E (2004). *Geophy. Res. Letts.*, 31, L17204, doi:10.1029/2004 GL020637.

Brill R W, and Lutcavage M E (2001). Understanding environmental factors influencing the depth distribution of tunas and billfish can significantly improve population assessments. *Am. Fish. Soc. Symp.*, 25, 179-198.

Brill R W, Bigelow K A, Musyl M K, Fritsches K A, and Warrant E J (2005). Bigeye tuna (*Thunnus obesus*) behavior and physiology and their relevance to stock assessments and fish biology. *Col. Vol. Sci. Pap. ICCAT* 57(2), 142-161.

Carton J A, Giese B S, and Grodsky S A (2005). Sea level rise and the warming of the oceans in the Simple Ocean Data Assimilation (SODA) ocean reanalysis. *J. Geophys. Res.*, 110(C9), doi:10.1029/2004JC002817.

Chavanne C, Flament P, Lumpkin R, Dousset B, Bentamy A (2002). Scatterometry observations of wind variations induced by oceanic islands: Implications for wind-driven ocean circulations. *Can J. Remote Sens.*, 28(3), 466-474.

Curran D, Boggs C, and He X (1996). Catch and effort in Hawaii's longline fishery summarized by quarters and five degrees squares. Honolulu Lab SWFC, NMFS, *NOAA Tech. Memo.* NOAA-TM-NMFS-SWFSC-225, 68 pp.

Dagorn L, Bach P, Josse E (2000). Movements patterns of large bigeye tuna (*Thunnus obesus*) in the open ocean, determined using ultrasonic telemetry. *Mar. Biol.*, 136, 361-371.

Firing E, Qiu B, and Miao W (1999). Time-dependant island rule and its application to the time varying north Hawaiian ridge current. *J. Phys. Ocean.*, 29, 2671-2688.

Firing, J, and Brainard R (2006). Ten years of shipboard ADCP measurements along the Northwestern Hawaiian Islands. *Atoll Res. Bull.*, 543, 347-364.

Flament P, Lumpkin C, and Firing E (1997). Current and eddy statistics for the Hawaii EEZ. *PFRP Newsletter*, v. 2, no. 3, July 1997.

Fu, L L, and Cazenave, A (2001). *Satellite altimetry and earth sciences: a handbook of techniques and applications*. Academic Press, San Diego, CA, 463 pp.

Gunn J, and Hampton J (2003). Migration and habitat preferences of bigeye tuina, Thunnus obesus, on the east coast of Australia. *Fisheries Develop. Corp. Milestone Prog. Rpt.*, (PP-0904), 24 pp.

Hampton J, Bigelow K, and Labelle M (1998). A summary of current information on the biology, fisheries and stock assessment of bigeye tuna (*Thunnus obesus*) in the Pacific Ocean, with recommendations for data requirements and future research. *Ocean Fisheries Tech. Prog. Tech. Rpt.*, no. 36, 45 pp.

Hampton J, and Gunn J (1998). Exploitation and movements of yellowfin tuna (*Thunnus albacares*) and bigeye tuna (*T. obesus*) tagged in the north-western Coral Sea. *Mar. Freshwater Res.*, 49, 475-489.

Hampton, J, Lewis A, and Williams P (1999). The western and central Pacific tuna fishery: 1998 overview and status of stocks. Sec Pacific Comm., *Oceanic Fish. Prog. Tuna Fish Assess. Rpt.*, no. 1, 39 pp.

Hampton J, Kleiber P, Langley A, Takeuchi Y, and Ichinokawa M (2005). Stock assessment of bigeye tuna in the western and central Pacific Ocean. *Proc. 1st Mtg. Scientific Comm. Western and Central Pacific Fish. Comm.* (WCPFC-SC1), August 2005.

Hanamoto E (1987). Effects of oceanographic environment on bigeye tuna distribution. *Bull. Japan Soc. Fish. Oceanogr*., 51, 203-216.

Holland C, and Mitchum G (2001). Propagation of big island eddies. *J. Geophys. Res.,* 106, C1, 935-944.

Howell E A, and Kobayashi D R (2006). El Nino effects in the Palmyra Atoll region; oceanographic changes and bigeye tuna (*Thunnus obesus*) catch rate variability. *Fish. Oceanogr.*, 15(6), 477-489.

IATTC (1999). Assessment of bigeye tuna in the eastern Pacific Ocean. Background paper 6, *Proc. 63rd Mtg. IATTC*, La Jolla, CA, 8-10 June.

Itano D, and Holland K (2000). Movement and vulnerability of bigeye (*Thunnus obesus*) and yellowfin tuna (*Thunnus albacares*) in relation to FADS and natural aggregation points. *Aquat. Living Resour.*, 13, 2000, 213-223.

Josse E, Bach P, Dagorn L (1998). Simultaneous observations of tuna movements and their prey by sonic tracking and acoustic surveys. *Hydrobiol.,* 371/372, 61-69.

Kobashi F and Kawamura H (2002). Seasonal variation and instability nature of the North Pacific Subtropical Countercurrent and the Hawaiian Lee Countercurrent. . *Geophys. Res.*, 107(C11), 10, DOI: 10.1029/2001JC001225.

Kume S (1967). Distribution and migration of bigeye tuna in the Pacific Ocean. *Rpt. Nankai Regional Fisheries Laboratory*, no. 255.

Lehodey P (2001). The pelagic ecosystem of the tropical Pacific Ocean: dynamic spatial modeling and biological consequences of ENSO. *Progr. Oceanogr.*, 49, 439-468.

Lehodey, P (2000). *Impacts of the El Niño Southern Oscillation on tuna populations and fisheries in the tropical Pacific Ocean*. Oceanic Fisheries Program, Secretariat of the Pacific Community, Noumea, New Caledonia, *Standing Comm. Tuna and Billfish*, SCTB 13.

Lehodey P, Bertignac M, Hampton J, Lewis A, and Pacaut J (1997). El Niño Southern Oscillation tuna in the western Pacific. *Nature*, 389, 16 October 1997.

Lumpkin R and Flament P (2001). Lagrangian statistics in the central North Pacific. *J. Mar. Syst.*, 29, 141-155.

Maunder M N, and Hoyle S D (2006). Status of bigeye tuna in the eastern Pacific Ocean in 2005 and the outlook for 2006. Working group to review stock assessments, *Proc. 7th Mtg. Inter American Trop. Tuna Comm.*, CA, May 2006.

Mitchum G (1995). The source of 90 day oscillations at Wake Island. *J. Geophys. Res.*, 100(C2), 2459-2475.

Miyabe N (1995). Follow up study on the stock status of bigeye tuna in the Pacific Ocean. *Fifth Mtg. Western Pacific Yellowfin Res. Group Working Paper 12*, Noumea, New Caledonia, 21-23 August, pp 15.

Musyl M K, Brill R W, Boggs C H, Curran D S, Kazama T K, and Seki M P (2003). Vertical movements of bigeye tuna (*Thunnus obesus*) associated with islands, buoys and seamounts near the main Hawaiian Islands from archival tags. *Fish. Oceanogr.*, 12:2, 1-18.

Nakano H, Okazaki M, Okamoto H (1997). Analysis of catch depth by species for tuna longline fishery based on catch by branch lines. *Bull. Nat. Res. Inst. Far Seas*. *Fish.*, no. 34, March 1997.

Patzert, W C (1969). Eddies in Hawaiian waters. *Office Naval Res. Tech. Rpt.*, 136 pp.

Qiu B, Koh D, Lumpkin C, and Flament P (1997). Existence and formation mechanism of the north Hawaiian ridge current. *J. Phys. Oceanogr.*, 27, 431-444.

Qiu B (1999) Seasonal eddy field modulation of the North Pacific subtropical countercurrent: Topex/Poseidon Observations and Theory. *J. Phys. Oceanogr.*, 29, 2471-2496.

RD Instruments (1998). Calculating absolute backscatter in narrowband ADCPs. *Field Tech. Paper 003* (FST-003), 01 May 1998.

Ressler P H (2002). Acoustic backscatter measurements with a 153kHz ADCP in the northeastern Gulf of Mexico: determination of dominant zooplankton and micro nekton scatterers. *Deep-Sea Res.*, 49, 2035-2051.

Roden, G I (1991). Subarctic subtropical transition zone of the North Pacific: large scale aspects and mesoscale structure. In Wetherall, J A (ed.), Biology, Oceanography and Fisheries of the North Pacific Transition Zone and Subarctic Frontal Zone, *NOAA Technical Report NMFS SWFSC 105*, p. 1-38.

Schaefer K M, and Fuller D W (2002). Movements, behavior and habitat selection of bigeye tuna (*Thunnus obesus*) in the eastern equatorial Pacific ascertained through archival tags. *Fish Bull.*, 100, 765-788.

Seki M, Polovina J, Brainard R, Bidigare R, Leonard C, and Foley D (2001). Biological enhancement at cyclonic eddies tracked with GOES thermal imagery in Hawaiian waters. *Geophys. Res. Letts.*, 28, 8, 1583-1586.

Seki M, Polovina J, Kobayashi D, Bidigare R, and Mitchum G (2002). An oceanographic characterization of Swordfish (*Xiphias gladius*) longline fishing grounds in the springtime subtropical North Pacific. *Fish. Oceanogr.*, 11:5, 251-266.

Sibert J, Hampton J, Kleiber P, and Maunder M (2006). Biomass, size and trophic status of top predators in the Pacific Ocean. *Science*, 314, 1773-1776.

Sibert J, Holland K, Itano D (2000). Exchange rates of yellowfin and bigeye tunas and fishery interaction between Cross Seamount and near-shore FADs in the Hawaii. *Aquat. Living Resour.*, 13, 225-232.

Sibert J, Musyl M, and Brill R (2003). Horizontal movements of bigeye tuna (*Thunnus obesus*) near Hawaii determined by Kalman filter analysis of archival tagging data. *Fish. Oceanogr.*, 12:3 141-151.

Smedstad O M, Hurlburt H E, Metzger E J, Rhodes R C, Shriver J F, Wallcraft A J, and Kara A B (2003). An operational eddy resolving 1/16° global ocean nowcast/forecast system. *J. Marine Syst.*, 40-41, 341-361.

Sun C L, Huang C L, Yeh S Z (2001). Age and growth of bigeye tuna, *Thunnus obesus*, in the western Pacific Ocean. *Fish. Bull.*, 99, 505-509.

Sund P, Blackburn M, and Williams F (1981). Tunas and their environment in the Pacific Ocean: A review. *Oceanogr. Mar. Biol. Ann. Rev.*, 1981, 19, 443-512.

Suzuki Z, Warashina Y, and Kishida M (1977). The comparison of catches by regular and deep tuna longline gears in the western and central equatorial Pacific. *Bull. Far Seas Fish. Res. Lab.* 15, 51-89.

Wilson C (2003) Late summer chlorophyll blooms in the oligotrophic North Pacific Subtropical Gyre. *Geophys. Res. Letts.*, 30, doi:10.1029/2003GL017770.

Xie S P, Liu W T, Liu Q, and Nonaka M (2001). Far reaching effects of the Hawaiian Islands on the Pacific Ocean-Atmosphere System. *Science*, 292, 2057-2060.

APPENDIX

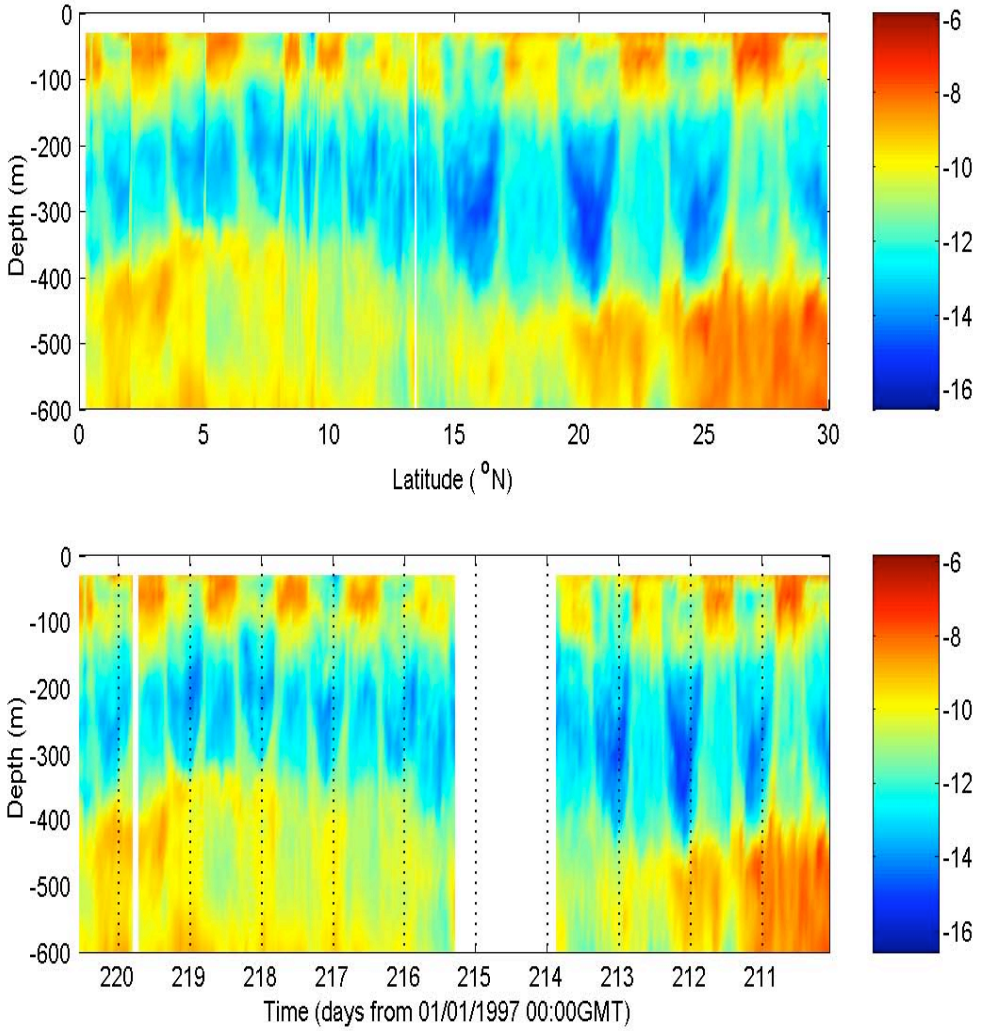

Figure A1. The volume backscatter, Sv, variation through depth with (a) latitude and (b) time for a cruise transect from 156°E 0°N to 141°E to 30°N on RV Kaiyo (JAMSTEC). Data were provided by the University of Hawaii from their ship-mounted ADCP database.

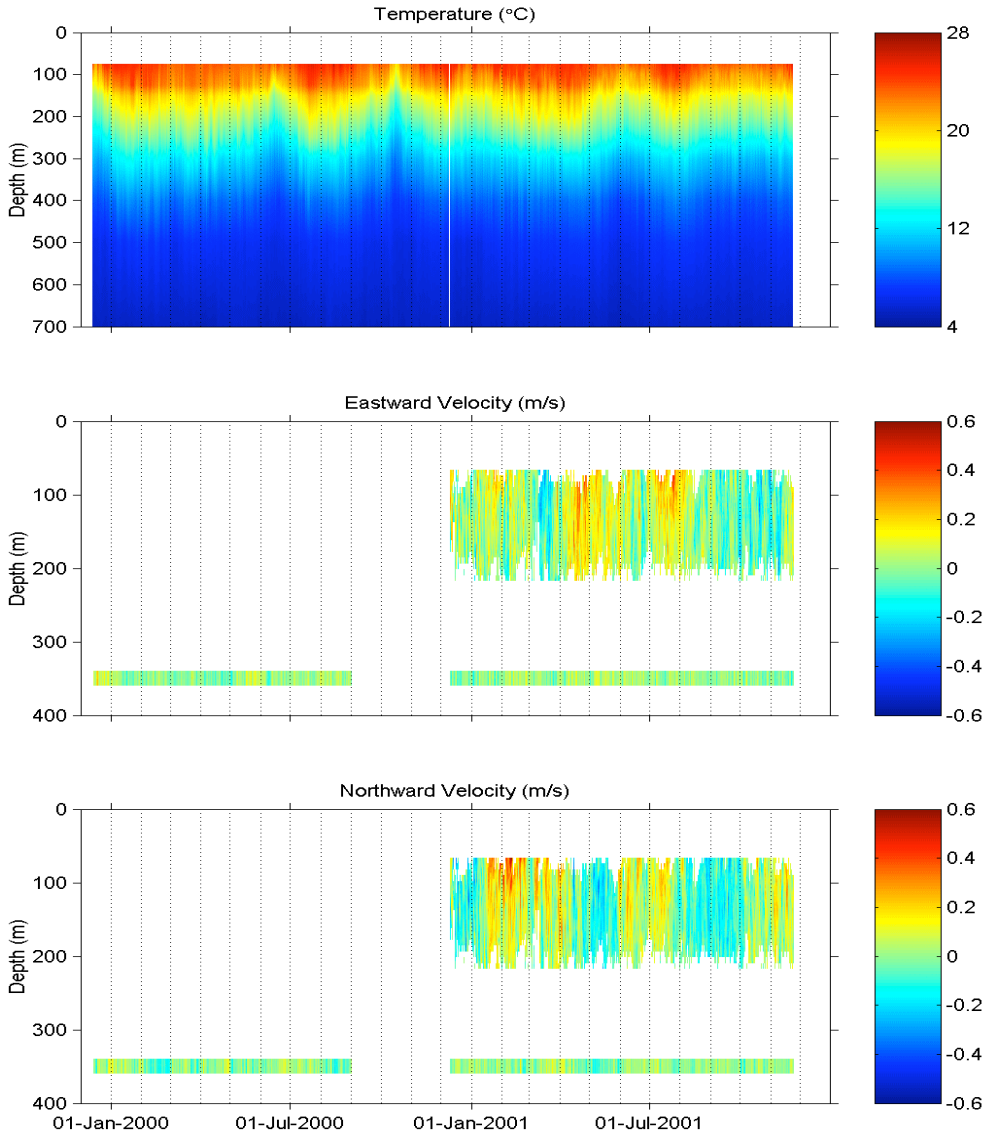

Figure A2. Temperature, eastward velocity and northward velocity variation at the Bigeye mooring location. Data are unfiltered. Note to allow visualization, current data from the RCM at 350 m depth have been duplicated at 340 and 360 m. The mooring recovery locations were 20.5993°N, 161.4251°W (Dec 1999 to Dec 2000) and 20.608°N, 161.580°W (Dec 2000 to Dec 2001). Water depth is 4735 m.

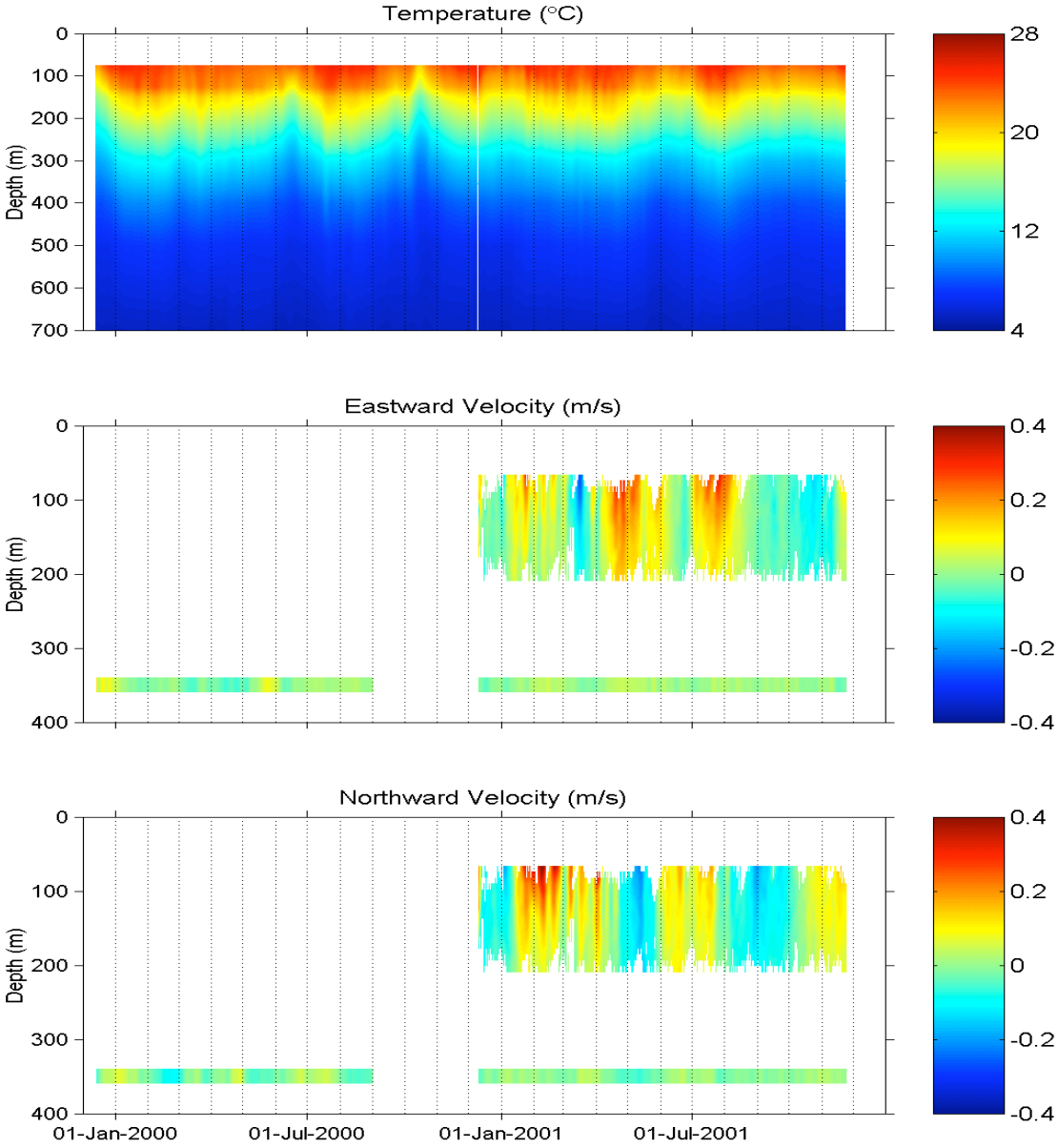

Figure A3. Temperature, eastward velocity and northward velocity variation at the mooring location. Data are filtered with a 96-hr low pass filter. Note to allow visualization, current data from the RCM at 350 m depth have been duplicated at 340 and 360 m. The mooring recovery locations were 20.5993°N, 161.4251°W (Dec 1999 to Dec 2000) and 20.608°N, 161.580°W (Dec 2000 to Dec 2001). Water depth is 4735 m.

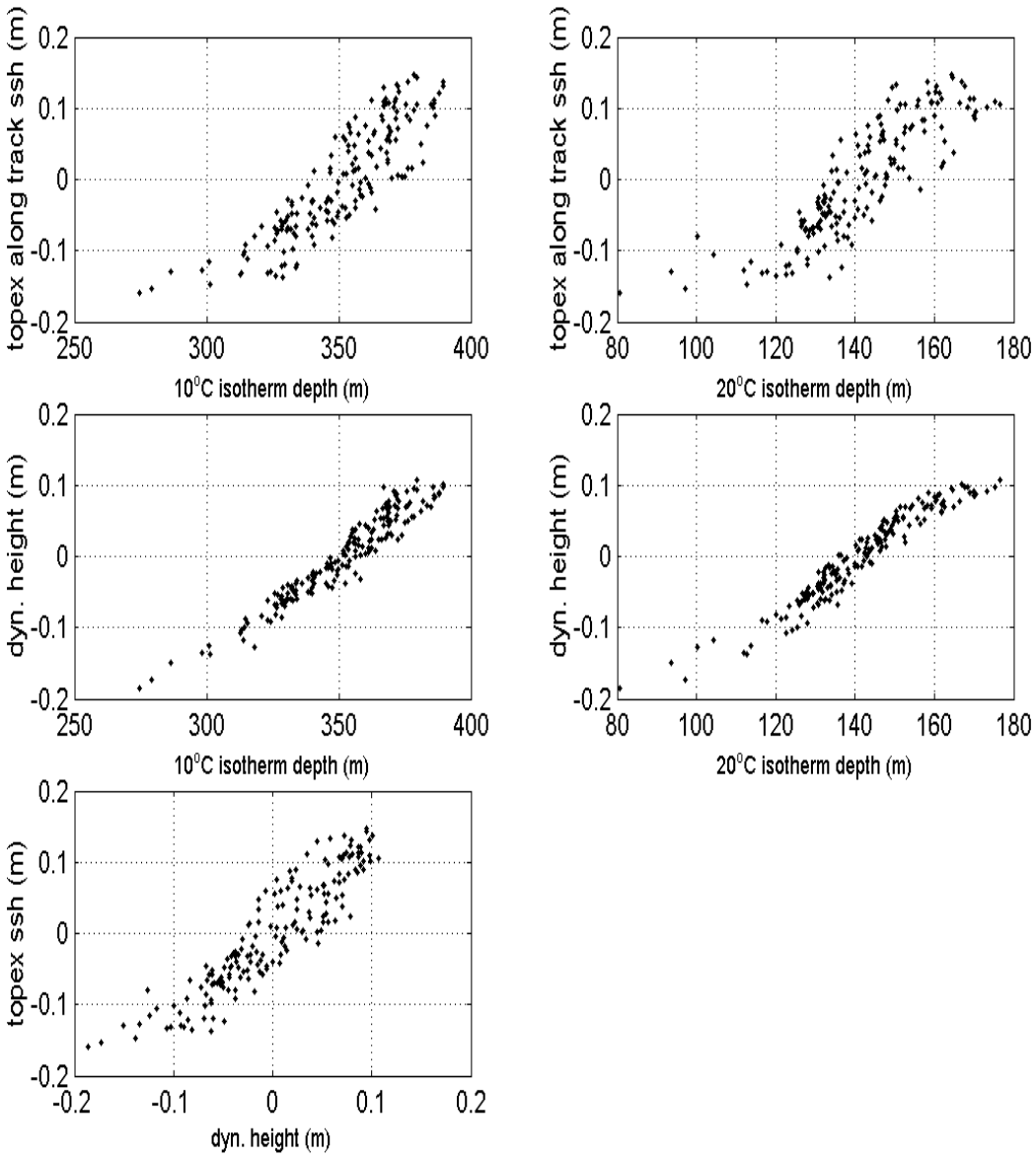

Figure A4. Correlation between 10°C isotherm depth, 20°C isotherm depth, sea surface height (from TOPEX along track observations) and dynamical height derived from the Bigeye mooring observations. Dynamic height is derived for the water column between 75 and 700 m depth from density calculated using salinity derived from temperature observations using a T-S relation from a CTD profile in December 2000.

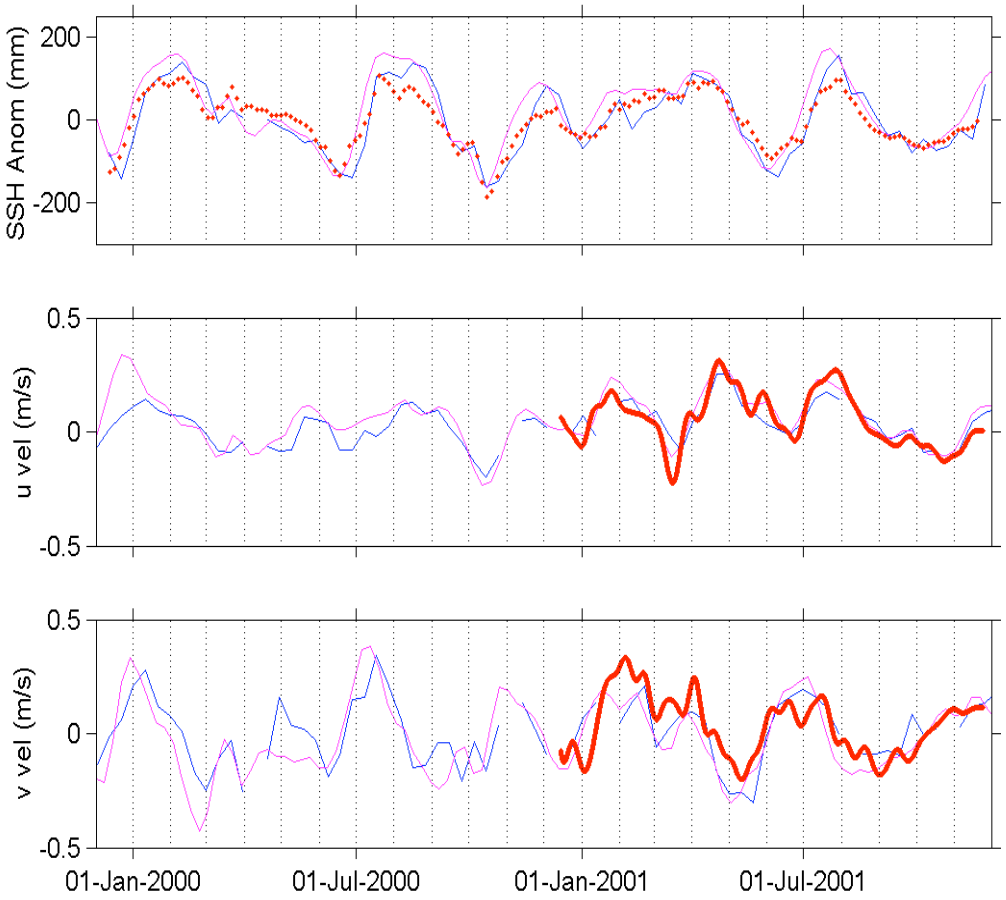

Figure A5. Sea surface height derived from along track (blue) and AVISO (magenta), and observed dynamic height (red). Dynamic height is calculated from observations of thermal structure between 75 m and 700 m from the bigeye mooring using salinity derived from the T-S relation in a CTD profile in December 2000. Along-track SSH is averaged from both up and down passes using data from 3 points either side of the altimeter crossover point at 20.615°N, 198.415°E. This corresponds to ± 0.06°E/W and ± 0.15°N/S. All SSH data are relative to mean level. (b) Eastward and northward current derived at the surface assuming geostrophic balance from the along track sea surface height (blue) and AVISO sea surface height (magenta) together with the observed velocities at 74 m from the ADCP (red). Note: AVISO data relative to mean sea level includes Levitus climatology sea surface height. The along track N/S and E/W gradients are calculated using locations 20 along track grid points on either side of the altimeter cross-over point where the mooring is located. This corresponds to a grid of ± 0.97°N/S (216 km distance) and ± 0.41°E/W (91 km distance). Along track data do not include Levitus climatology sea surface height and therefore do not include the mean flow.

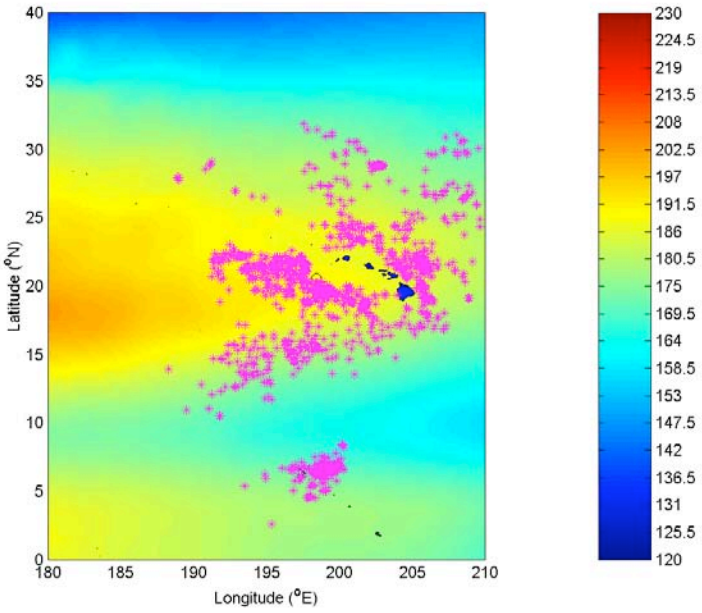

Figure A6. Annual mean sea surface elevation (cm) derived from Levitus sea surface height (WOA01) data. The plot is mean of AVISO sea level anomaly plus local mean sea surface elevation (Levitus) from 1992 to 2003. Locations of CPUE in excess of 20 fish per thousand hooks are indicated with magenta stars.

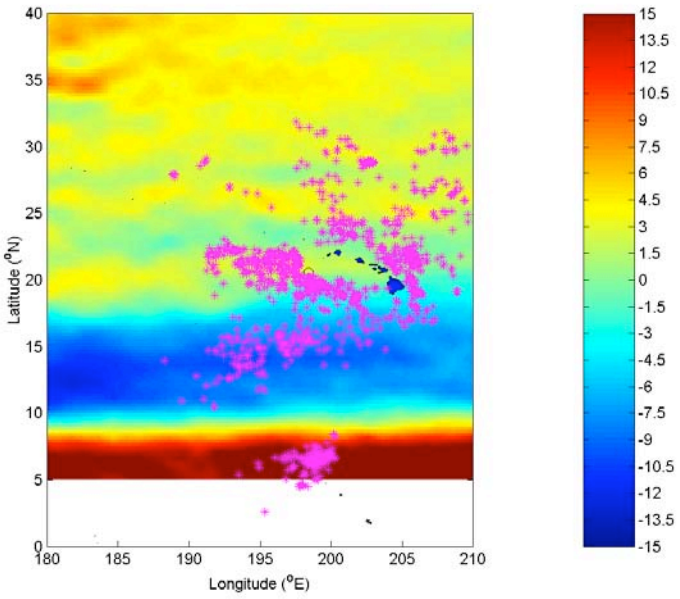

Figure A7. Annual mean eastward geostrophic velocity component (cm/s) derived from AVISO sea surface elevation anomaly plus mean local sea surface elevation from 1992 to 2003. Locations of CPUE in excess of 20 fish per 1000 hooks are indicated with magenta stars.

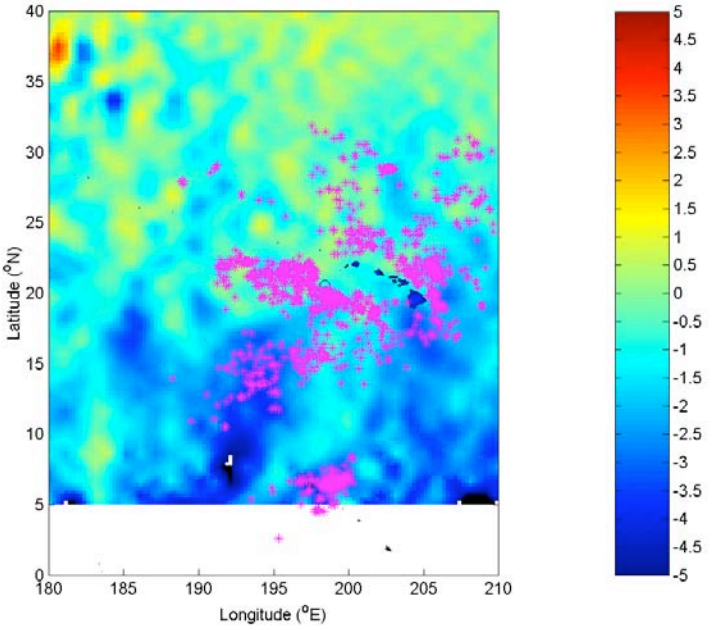

Figure A8. Annual mean northward geostrophic velocity component (cm/s) derived from AVISO sea surface elevation anomaly plus mean local sea surface elevation from 1992 to 2003. Locations of CPUE in excess of 20 fish per 1000 hooks are indicated with magenta stars.

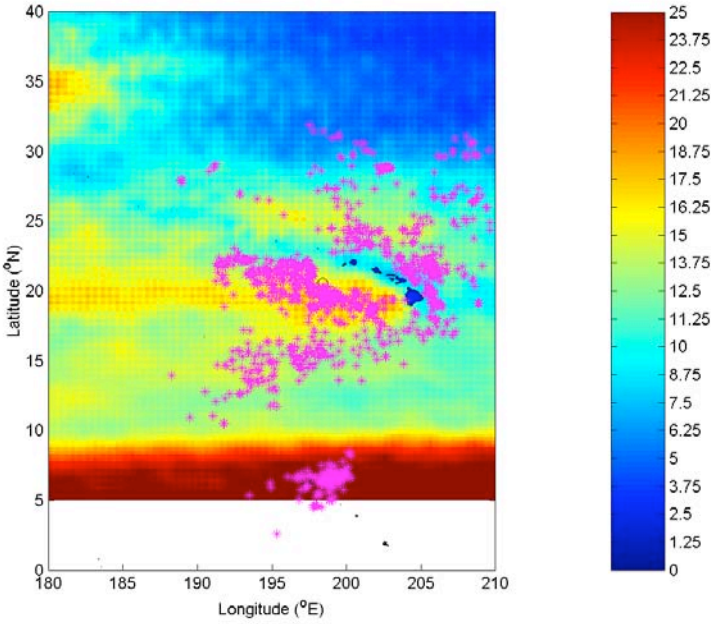

Figure A9. Annual mean geostrophic current speed (cm/s) derived from AVISO sea surface elevation anomaly plus mean local sea surface elevation from 1992 to 2003. Locations of CPUE in excess of 20 fish per 1000 hooks are indicated with magenta stars.

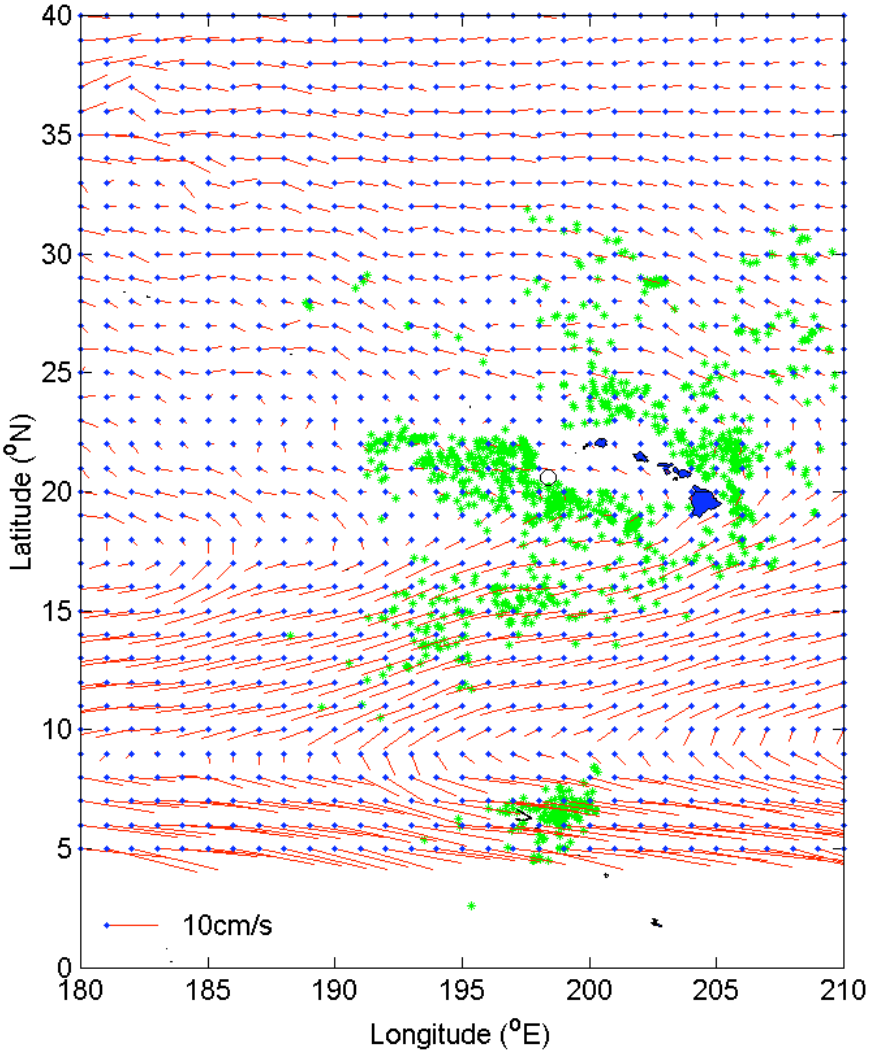

Figure A10. Annual mean geostrophic current vectors (cm/s) derived from AVISO sea surface elevation anomaly plus mean local sea surface elevation from 1992 to 2003. Locations of CPUE in excess of 20 fish per 1000 hooks are indicated with green stars.

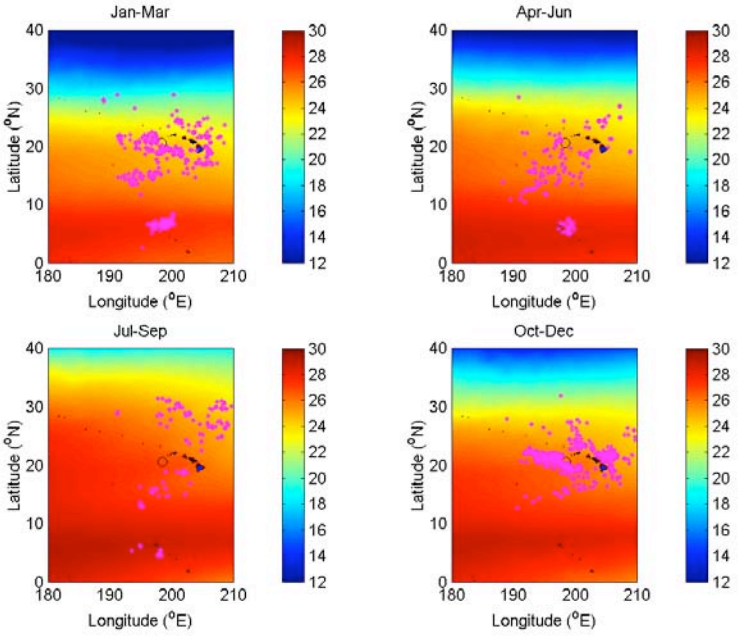

Figure A11. Seasonal mean sea surface temperature (°C) derived from satellite observations from 1992 to 2003. Locations of CPUE in excess of 20 fish per 1000 hooks are indicated with magenta stars.

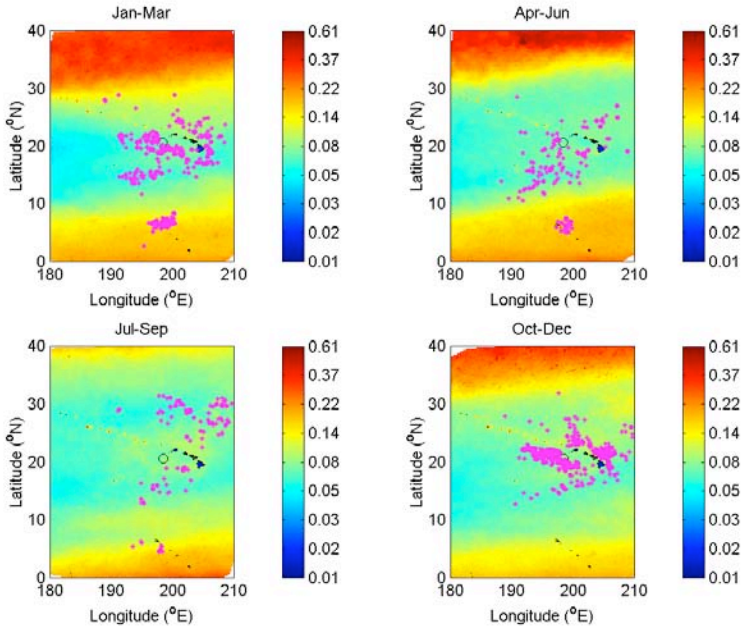

Figure A12. Seasonal mean sea surface chlorophyll (mg/l) derived from satellite observations from 1992 to 2003. Locations of CPUE in excess of 20 fish per 1000 hooks are indicated with magenta stars. Note a logarithmic color scale is used.

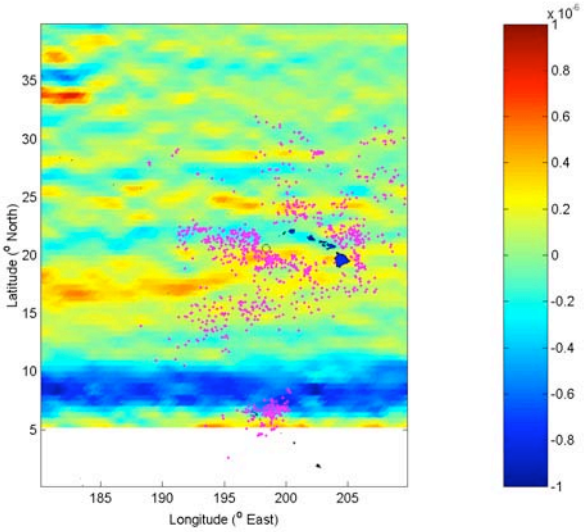

Figure A13. Annual mean eastward geostrophic current convergence (du/dx) derived from AVISO sea surface elevation anomaly plus mean local sea surface elevation from 1992 to 2003. Locations of CPUE in excess of 20 fish per 1000 hooks are indicated with magenta stars. Note since geostrophic currents are by definition non-divergent this should be identical (but opposite sign) to the equivalent figure for the northward component.

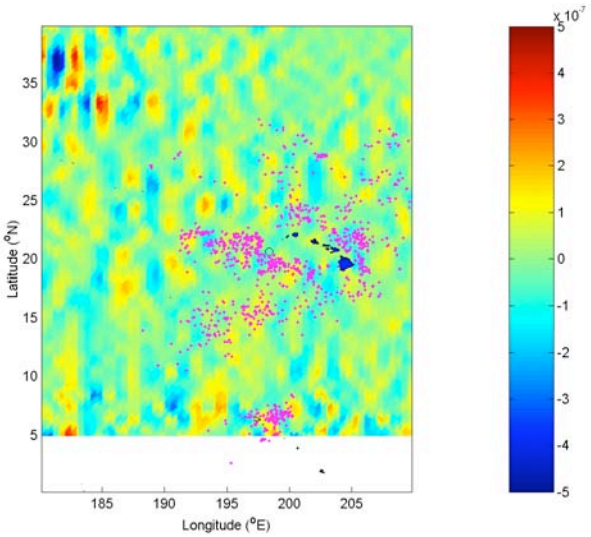

Figure A14. Annual mean northward geostrophic current convergence (dv/dy)) derived from AVISO sea surface elevation anomaly plus mean local sea surface elevation from 1992 to 2003. Locations of CPUE in excess of 20 fish per 1000 hooks are indicated with magenta stars. Note the apparent evidence of satellite track lines indicating errors as expected for a second derivative of an interpolated parameter. Note since geostrophic currents are by definition non-divergent this should be identical but opposite sign to the equivalent figure for the eastward component.

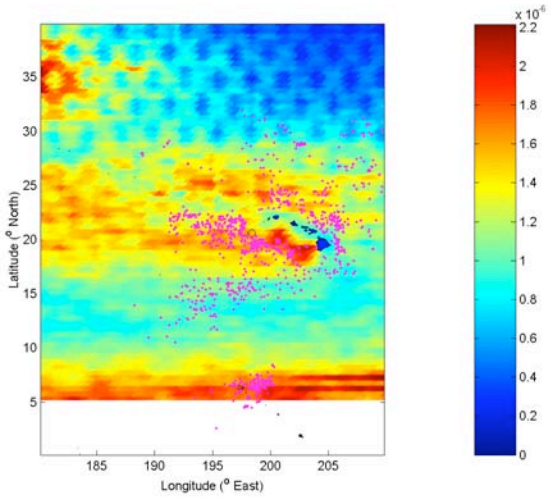

Figure A15. Annual mean absolute eastward geostrophic current convergence (abs(du/dx)) derived from AVISO sea surface elevation anomaly plus mean local sea surface elevation from 1992 to 2003. Locations of CPUE in excess of 20 fish per 1000 hooks are indicated with magenta stars. Note the evidence of satellite track lines indicating errors as expected for a second derivative of an interpolated parameter. Note since geostrophic currents are by definition non-divergent this should be identical but opposite sign to equivalent figure for the northward component.

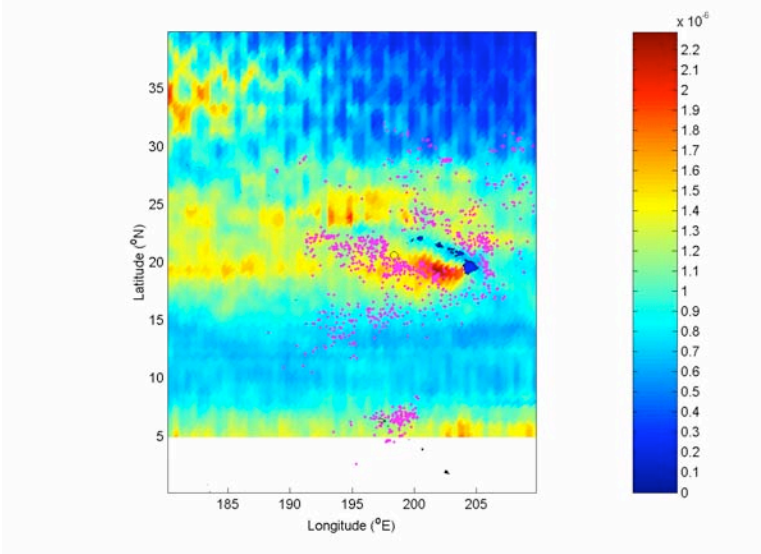

Figure A16. Annual mean absolute northward geostrophic current convergence (abs(dv/dy)) derived from AVISO sea surface elevation anomaly plus mean local sea surface elevation from 1992 to 2003. Locations of CPUE in excess of 20 fish per 1000 hooks are indicated with magenta stars. Note the evidence of satellite track lines indicating errors as expected for a second derivative of an interpolated parameter. Note since geostrophic currents are by definition non-divergent this should be identical but opposite sign to equivalent figure for the eastward component.

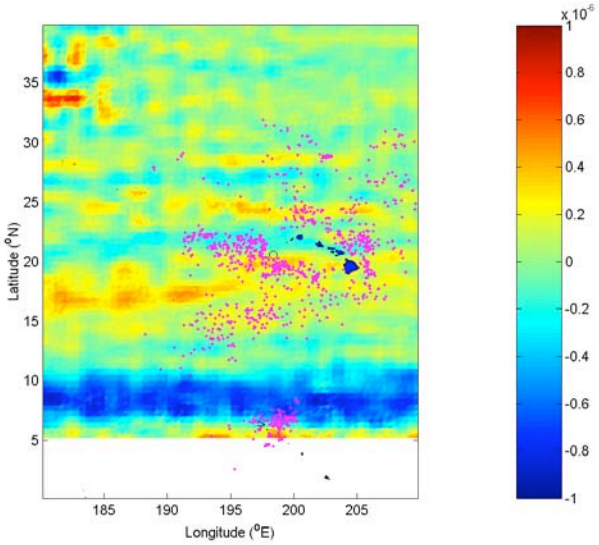

Figure A17. Annual mean geostrophic current convergence (du/dx + dv/dy) derived from AVISO sea surface elevation anomaly plus mean local sea surface elevation from 1992 to 2003. Locations of CPUE in excess of 20 fish per 1000 hooks are indicated with green stars. Note the evidence of satellite track lines indicating errors as expected for a second derivative of an interpolated parameter. Also note since geostrophic currents are by definition non-divergent this should be zero.

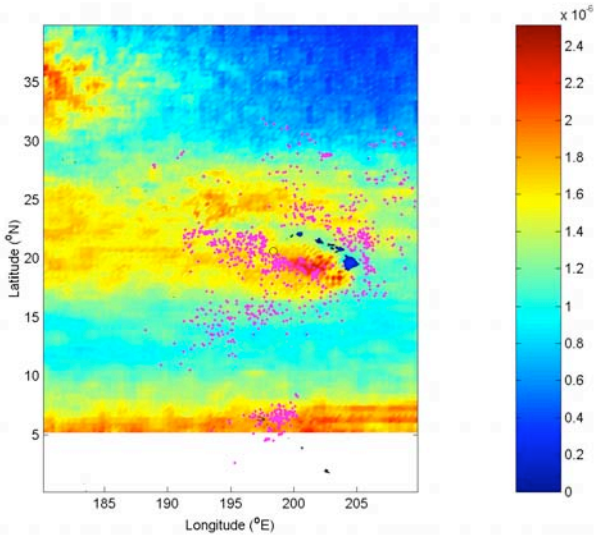

Figure A18. Annual mean absolute geostrophic current convergence (abs(du/dx + dv/dy)) derived from AVISO sea surface elevation anomaly plus mean local sea surface elevation from 1992 to 2003. Locations of CPUE in excess of 20 fish per 1000 hooks are indicated with green stars. Note the evidence of satellite track lines indicating errors as expected for a second derivative of an interpolated parameter. Also note since geostrophic currents are by definition non-divergent this should be zero.

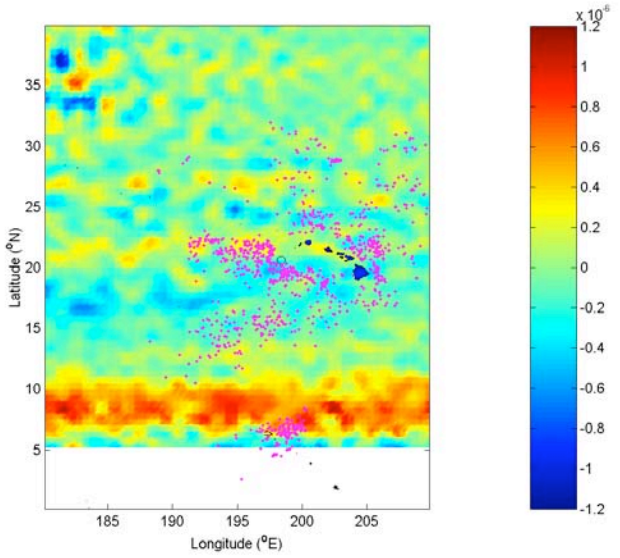

Figure A19. Annual mean absolute geostrophic current vorticity (dv/dx–du/dy)) derived from AVISO sea surface elevation anomaly plus mean local sea surface elevation from 1992–2003. Locations of CPUE in excess of 20 fish per thousand hooks are indicated with magenta stars. Note the possible evidence of banding aligned with satellite track lines indicating errors as expected for a second derivative of an interpolated parameter.

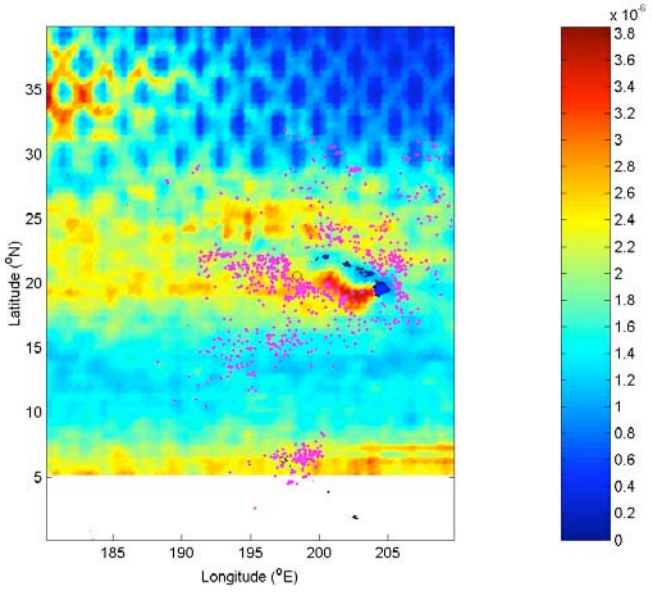

Figure A20. Annual mean absolute geostrophic current vorticity (abs(du/dy–dv/dx)) derived from AVISO sea surface elevation anomaly plus mean local sea surface elevation from 1992–2003. Locations of CPUE in excess of 20 fish per thousand hooks are indicated with magenta stars. Note the evidence of satellite track lines indicating errors as expected for a second derivative of an interpolated parameter.

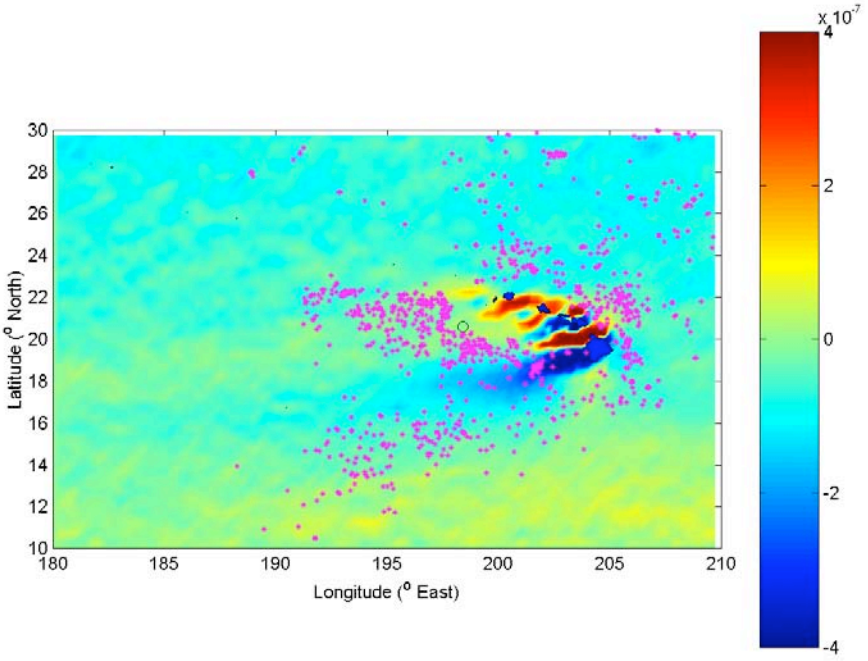

Figure A21. Annual mean wind stress (Pa) vorticity (dv/dx–du/dy) derived from QSCAT satellite observations between 1999 and 2003. Locations of CPUE in excess of 20 fish per thousand hooks are indicated with magenta stars.

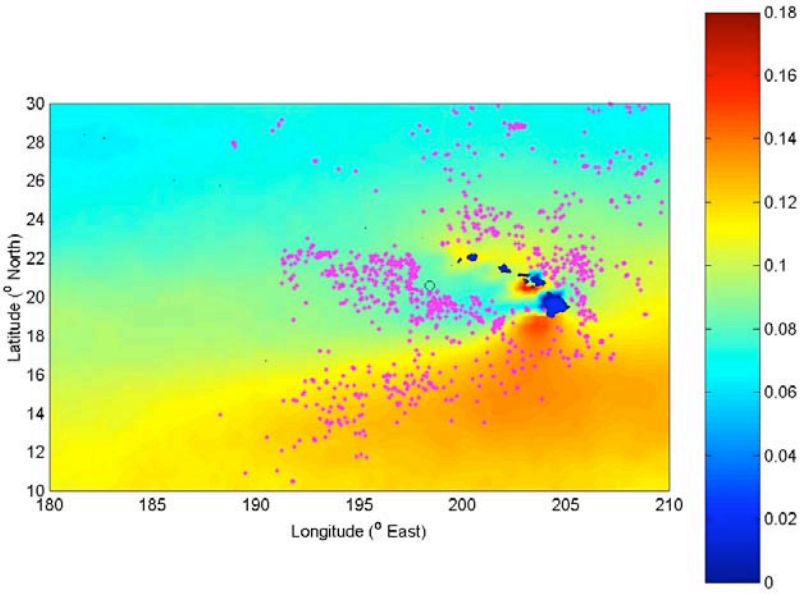

Figure A22. Annual mean total wind stress (Pa) derived from QSCAT satellite observations between 1999 and 2003. Locations of CPUE in excess of 20 fish per thousand hooks are indicated with magenta stars.

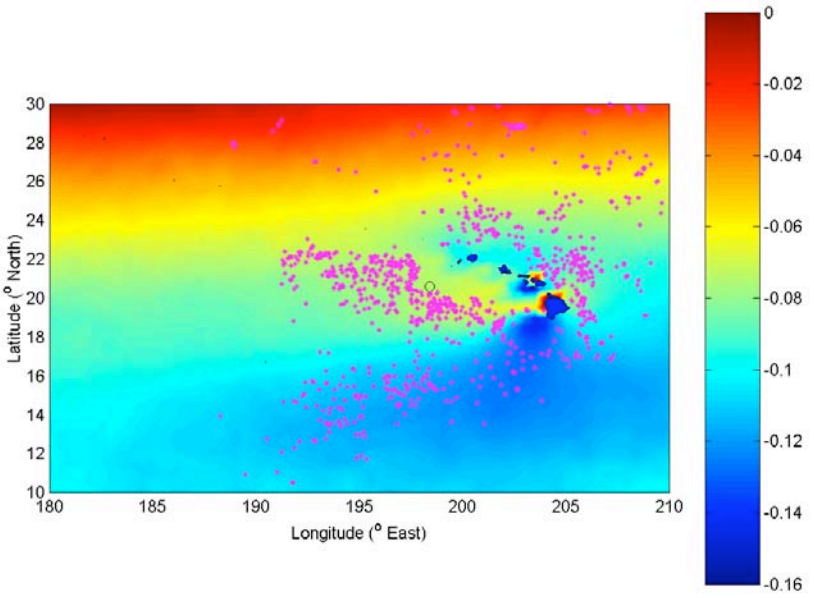

Figure A23. Annual mean eastward wind stress (Pa) derived from QSCAT satellite observations between 1999 and 2003. Locations of CPUE in excess of 20 fish per 1000 hooks are indicated with magenta stars.

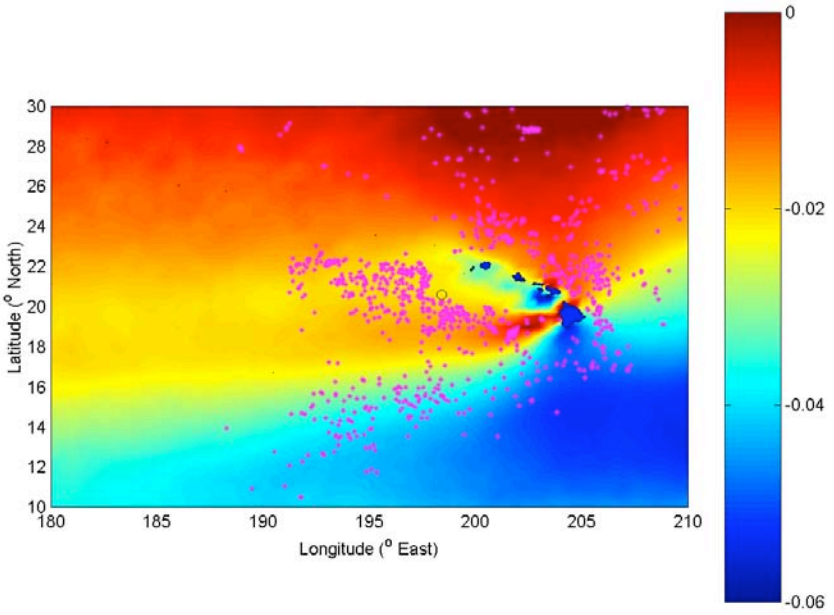

Figure A24. Annual mean northward wind stress (Pa) derived from QSCAT satellite observations between 1999 and 2003. Locations of CPUE in excess of 20 fish per 1000 hooks are indicated with magenta stars.

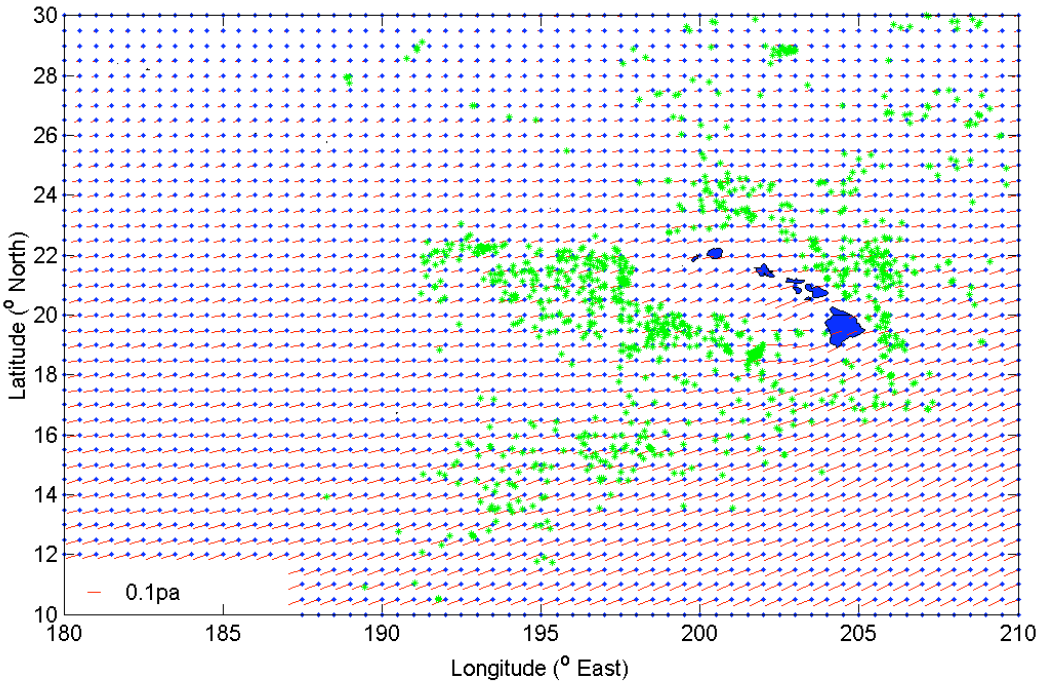

Figure A25. Annual mean wind stress (Pa) vectors derived from QSCAT satellite observations between 1999 and 2003. Locations of CPUE in excess of 20 fish per 1000 hooks are indicated with green stars.

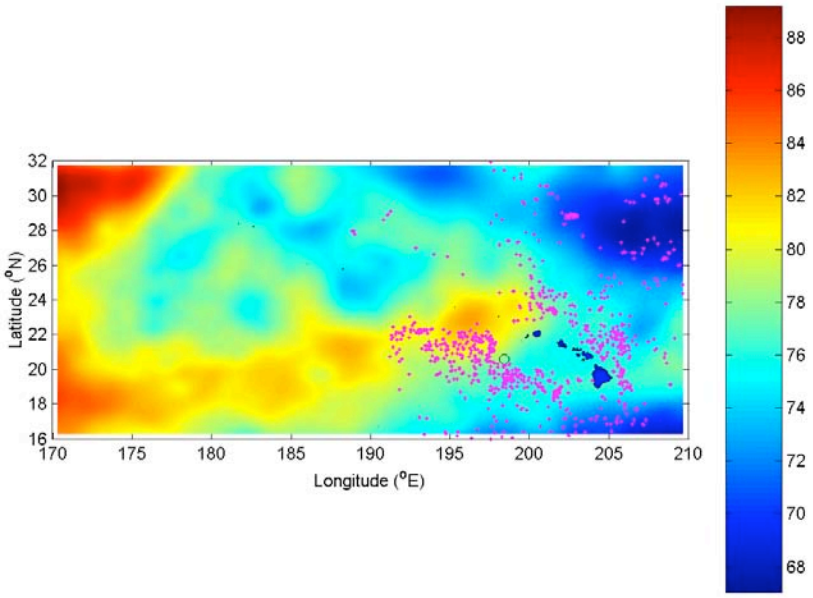

Figure A26. Annual mean sea surface height (cm) from the NLOM model for 2001. Locations of CPUE in excess of 20 fish per 1000 hooks are indicated with magenta stars.

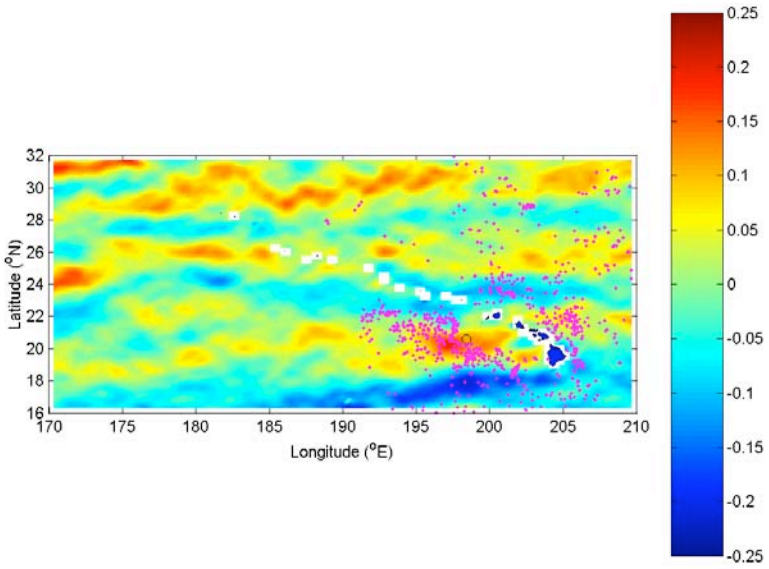

Figure A27. Annual mean upper layer (~0–64 m) eastward current (m/s) from the NLOM model for 2001. Locations of CPUE in excess of 20 fish per 1000 hooks are indicated with magenta stars.

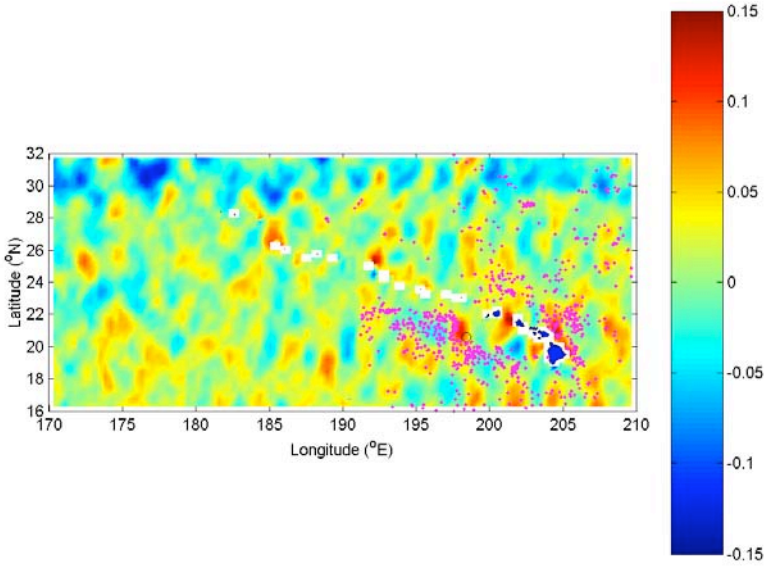

Figure A28. Annual mean upper layer (~0–64 m) northward current (m/s) from the NLOM model for 2001. Locations of CPUE in excess of 20 fish per 1000 hooks are indicated with magenta stars. Note banding structure that has similar alignment to altimeter pass lines. This could suggest assimilation of interpolated sea surface height fields results in errors in model currents.

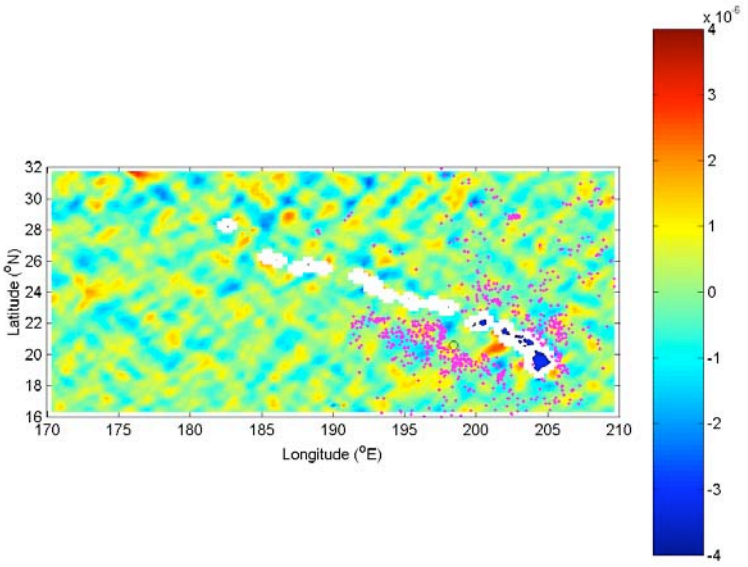

Figure A29. Annual mean upper layer (~0–64 m) current vorticity (dv/dx–du/dy) from the NLOM model for 2001. Locations of CPUE in excess of 20 fish per 1000 hooks are indicated with magenta stars. Note banding structure that has similar alignment to altimeter pass lines. This could suggest assimilation of interpolated sea surface height fields results in errors in model currents.

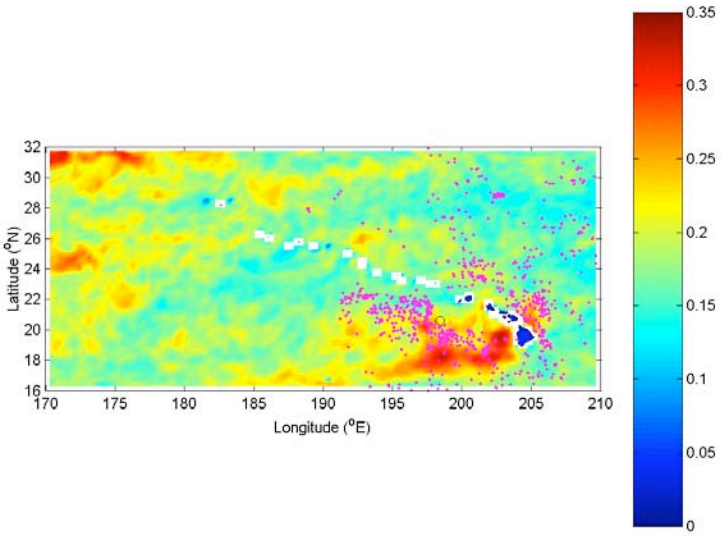

Figure A30. Annual mean upper layer (~0–64 m) current speed from the NLOM model for 2001. Locations of CPUE in excess of 20 fish per 1000 hooks are indicated with magenta stars.

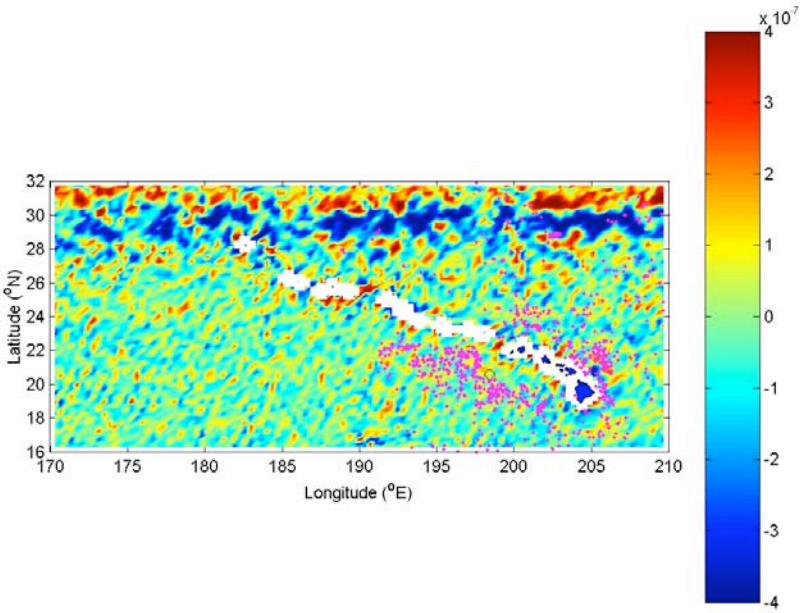

Figure A31. Annual mean upper layer (~0–64 m) current convergence from the NLOM model for 2001. Locations of CPUE in excess of 20 fish per 1000 hooks are indicated with magenta stars.

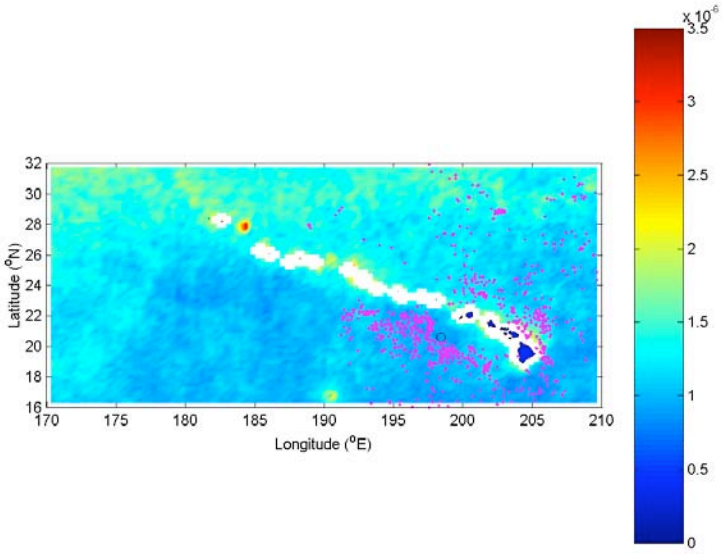

Figure A32. Annual mean upper layer (~0–64 m) current absolute convergence from the NLOM model for 2001. Locations of CPUE in excess of 20 fish per 1000 hooks are indicated with magenta stars.

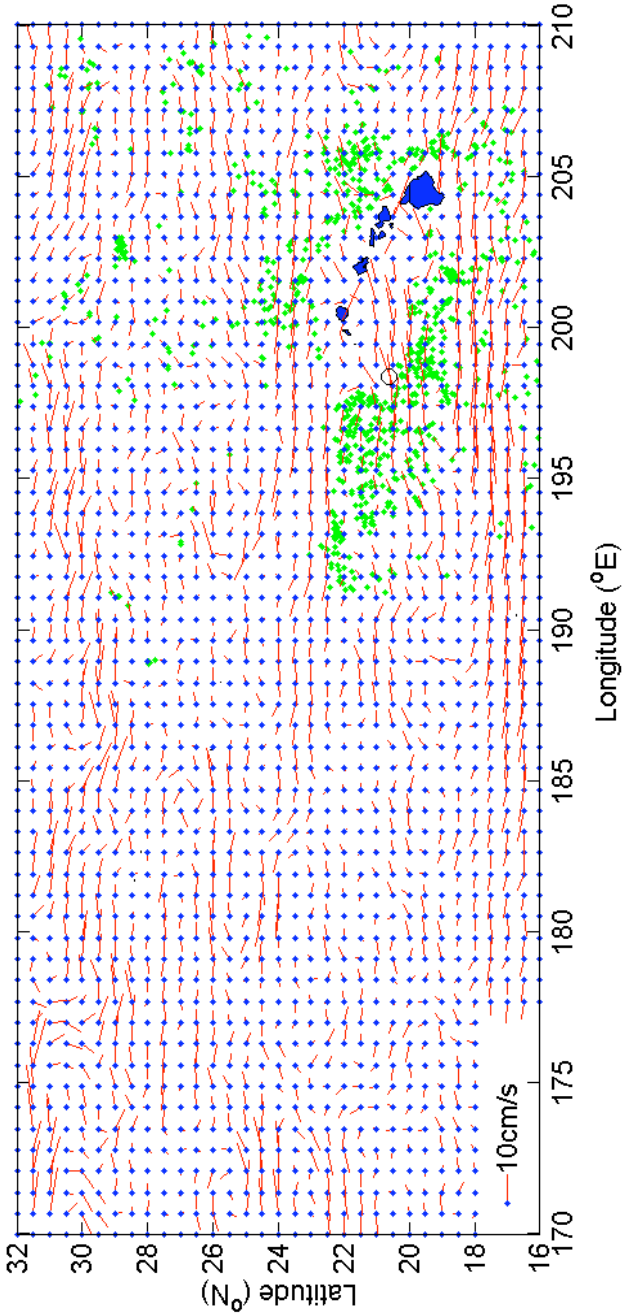

Figure A33. Annual mean upper layer (~0–64 m) current vectors from the NLOM model for 2001. Locations of CPUE in excess of 20 fish per 1000 hooks are indicated with green stars. Note these currents include estimates of the upper layer Ekman transport (unlike geostrophic currents).

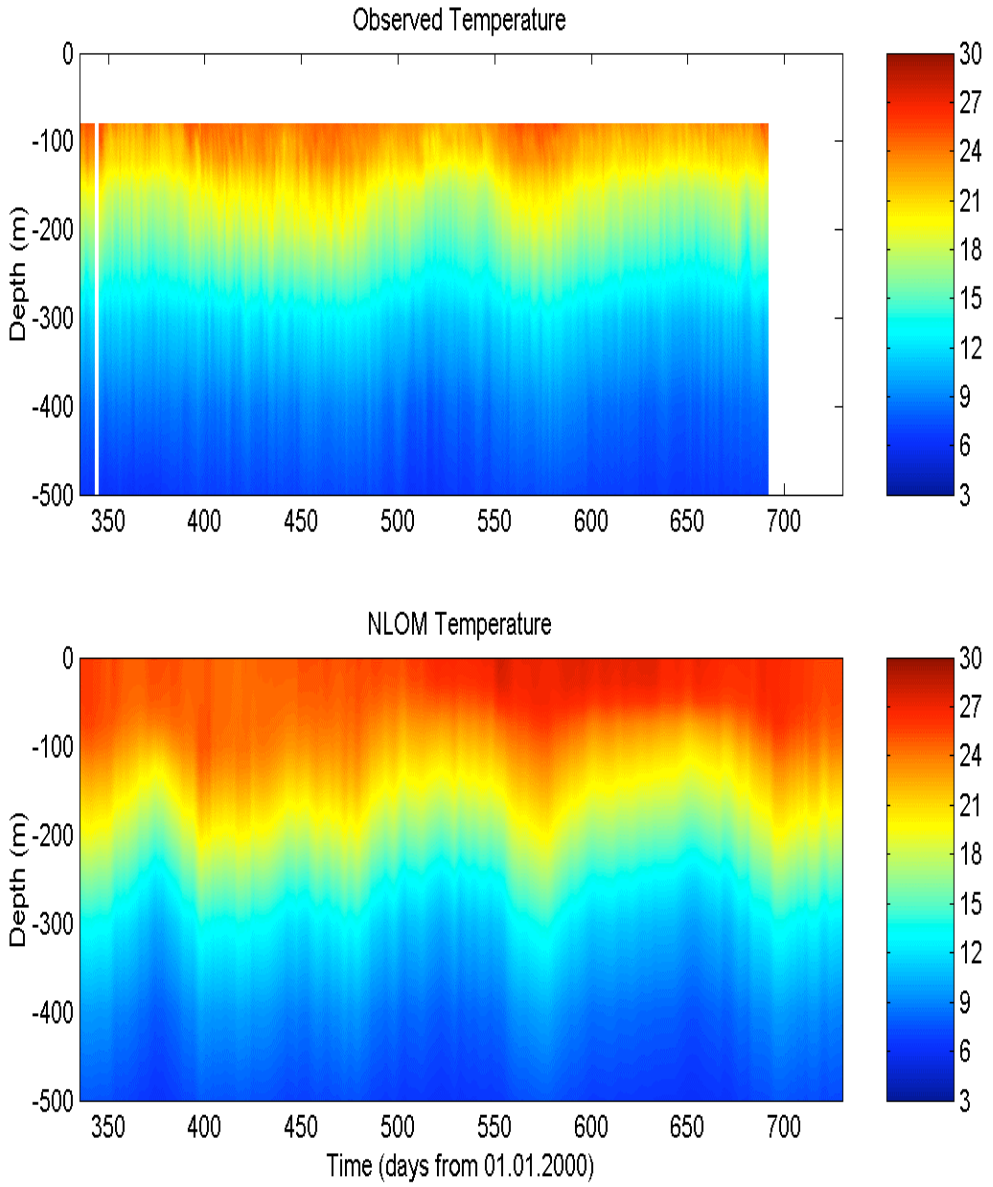

Figure A34. Temperature in the upper 500 m of the water column at the mooring location from subsurface instruments and from the NLOM model. Note: although the NLOM model is only seven layers, high-resolution temperature profiles are regenerated by the model using a statistical technique.

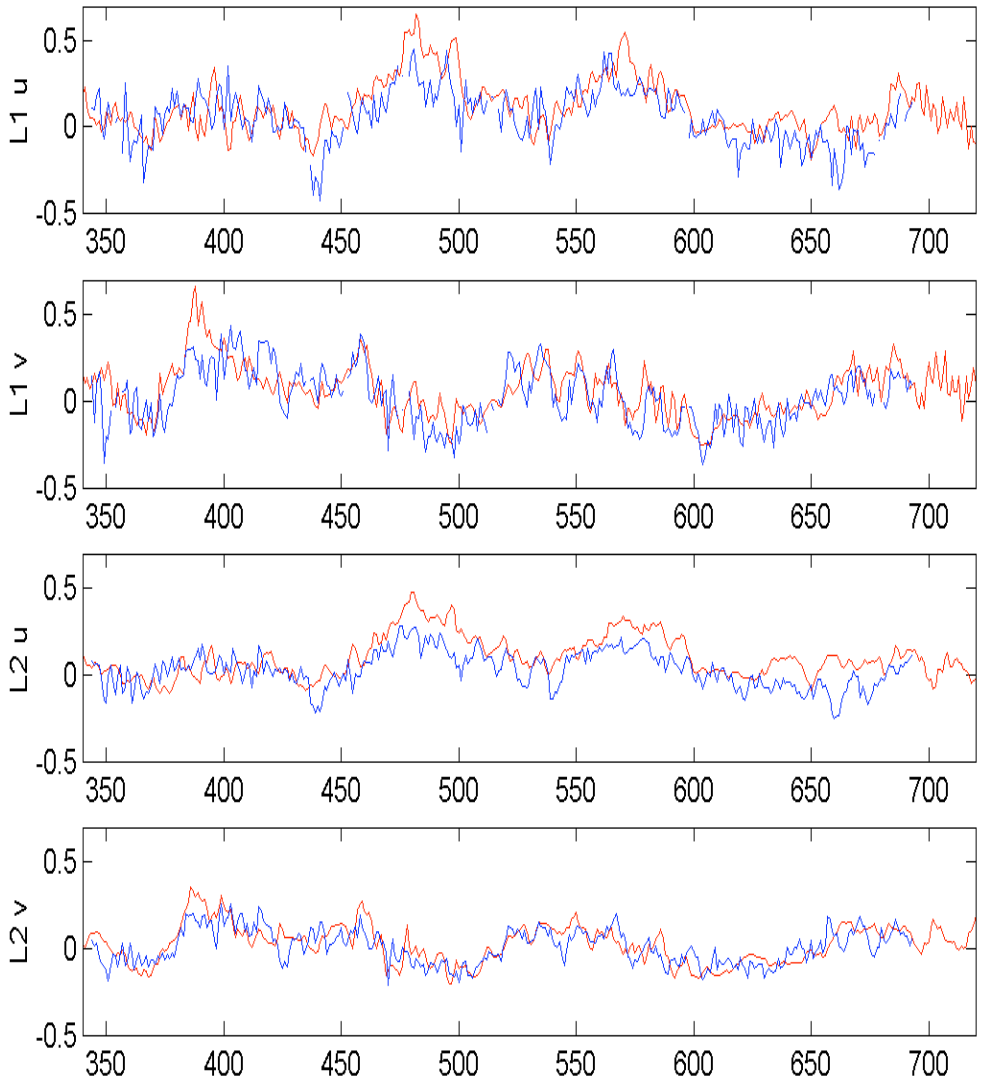

Figure A35. Layer 1 and Layer 2 eastward and northward current (m/s) from the NLOM model (red) and observed by the ADCP (blue) at the mooring location. NLOM layers vary in depth but their mean thicknesses are 64, 238, and 302 m for the upper three layers corresponding to 0–64 m, 64–302 m and 302–604 m. For comparison with Layer 1 we used the closest ADCP observations, which are at 74 m. For comparison with Level 2 we use the mean of ADCP observations between 74 m and 218 m.